Lithos xxx (2013) xxx–xxx

Contents lists available at SciVerse ScienceDirect

Lithos

journal homepage: www.elsevier.com/locate/lithos

Petrogenesis of serpentinites from the Franciscan Complex, western California, USA

Jaime D. Barnes [a,*], Rania Eldam [a], Cin-Ty A. Lee [b], Jessica C. Errico [a], Staci Loewy [a], Miguel Cisneros [a]

[a] Department of Geological Sciences, University of Texas, Austin, TX 78712, USA
[b] Department of Earth Science, MS-126, Rice University, Houston, TX 77005, USA

ARTICLE INFO

Article history:
Received 1 September 2012
Accepted 8 December 2012
Available online xxxx

Keywords:
Serpentinite
Franciscan Complex
Coast Range ophiolite
Stable isotope
Trace element

ABSTRACT

Serpentinites from the Franciscan Complex of California, USA, were analyzed for their bulk major and trace element compositions, relict mineral (spinel and pyroxene) compositions, and stable isotope (O, H, Cl) compositions with the goal of determining protolith origin and subsequent serpentinizing fluid sources in order to decipher the tectonic setting of serpentinization. We focused on serpentinite bodies found in the Franciscan Complex (west of Cuesta Ridge; south of San Francisco; Tiburon Peninsula; Healdsburg) ($n = 12$). Three samples from Cuesta Ridge (part of the Coast Range ophiolite) were also analyzed for comparison. Serpentinites from Cuesta Ridge have flat to U-shaped chondrite-normalized REE patterns and spinels with Cr# values >0.60 implying a supra-subduction zone origin. In contrast, Franciscan serpentinites west of Cuesta Ridge and Tiburon Peninsula have positive-sloped REE patterns. This depletion in LREE is typical of abyssal peridotites. Most relict spinels have low Cr# values (<0.3) and relict clinopyroxenes from Tiburon Peninsula have high HREE concentrations, also supporting an abyssal origin. Franciscan serpentinite samples from south of San Francisco and near Healdsburg have U-shaped REE patterns and spinel compositions that lie within the forearc peridotite field with some overlap into the abyssal field and are of more ambiguous origin. All samples are high in fluid-mobile elements with remarkable positive Ce and Y anomalies. We speculate that these anomalies may be due to involvement of highly oxidizing fluids resulting in the preferential scavenging of Ce and Y by ferromanganese oxyhydroxides during serpentinization. All samples (except those south of San Francisco) have $\delta^{18}O$ values of $+5.4$ to $+7.9‰$, typical values for oceanic serpentinites formed via low-T seawater hydration on the seafloor. δD values of all samples are extremely low (-107 to $-90‰$), likely the result of post-serpentinization, post-emplacement interaction with meteoric water at low temperature. Samples south of San Francisco lie on the San Andreas fault and have high $\delta^{18}O$ values ($+7.2$ to $+9.5‰$) likely due to low-T interaction with meteoric water at high fluid–rock ratios. Most of the serpentinites have $\delta^{37}Cl$ values between $+0.2$ and $+0.9‰$, typical values for serpentinites formed by interaction with seawater. Exceptions are those from the San Andreas fault and one sample from Cuesta Ridge with a high $\delta^{37}Cl$ value ($+1.7‰$) possibly from interaction with a slab-derived fluid.

1. Introduction

Serpentinites are formed in many different geologic settings, such as off-axis fractures and faults associated with seafloor spreading ridges, hydrated mantle wedge above a subducting slab (supra-subduction zone, SSZ), within the subduction channel, and along flexural faults associated with plate bending during subduction (e.g., Dilek, 2003; Ranero et al., 2003). In many cases, obducted serpentinites (and associated ophiolitic units) are highly dismembered and deformed making tectonic interpretation of the origin of these rocks difficult. Determining the geologic setting of serpentinization is critical to addressing tectonic questions and quantifying geochemical fluxes.

Due to the preferential partitioning of H_2O and fluid mobile elements (FME, e.g., Cl, F, B, S, As, Sb, Pb, Ni, Cr) into serpentinites, serpentinites act as a record of fluid history. Different modes of hydration and sources of serpentinizing fluids (e.g., seawater vs. slab-derived) reflect different tectonic settings of serpentinization and create variations in the resulting serpentinite geochemistry (Kodolánya et al., 2012). In general, serpentinization is isochemical with respect to the major elements, with the exception of CaO loss; however, the behavior of trace elements is not as well constrained (Mével, 2003). MgO can be lost due to low-temperature (<150 °C) marine weathering on the seafloor (Snow and Dick, 1995) and interaction with high temperature fluids from hydrothermal systems can also result in mobility of some LREE (Eu and Ce), as

* Corresponding author.
E-mail address: jdbarnes@jsg.utexas.edu (J.D. Barnes).

0024-4937/$ – see front matter © 2013 Elsevier B.V. All rights reserved.
http://dx.doi.org/10.1016/j.lithos.2012.12.018

well as, Si, Fe, Cr, and Ni (e.g., Augustin et al., 2012; Douville et al., 2002; Janecky and Seyfried, 1986; Paulick et al., 2006). Despite original geochemical heterogeneities in the protolith, major- and trace-element chemistry has been used to identify the tectonic setting of serpentinization (e.g., Dai et al., 2011; Deschamps et al., 2010; Hattori and Guillot, 2007; John et al., 2010b; Li and Lee, 2006). For example, SSZ serpentinites are characterized by low Al/Si weight ratios (<0.03), enrichments in FME compared to abyssal peridotites, U-shaped REE patterns, and slight enrichments in LREE relative to HFSE. In contrast, abyssal peridotites have moderate Al/Si ratios (>0.03) and low LREE concentrations (Agranier et al., 2007; Deschamps et al., 2010, 2011; Hattori and Guillot, 2007; John et al., 2010b; Kodolánya et al., 2012; Li and Lee, 2006; Niu, 2004; Savov et al., 2005, 2007). However, melt refertilization in a MOR setting can also result in LREE enrichments in abyssal peridotites creating U-shaped REE patterns (Niu, 2004; Paulick et al., 2006).

In addition, stable isotopes (O, H, Cl, Li, B) are effective tracers of serpentinizing fluid sources and post-serpentinite fluid interaction (Alt and Shanks, 2006; Barnes and Sharp, 2006; Barnes et al., 2006, 2009; Benton et al., 2001, 2004; Burkhard and O'Neil, 1988; Cartwright and Barnicoat, 1999; Früh-Green et al., 1990, 1996, 2001; Kyser et al., 1999; Sakai et al., 1990; Skelton and Valley, 2000; Tonarini and Scambelluri, 2010; Vils et al., 2009; Yui et al., 1990). The final isotopic composition of the serpentinite will be determined by the isotopic composition of the serpentinizing fluid, the temperature of interaction, and the water/rock ratio. For example, high $\delta^{18}O$ values may be the result of low-temperature serpentinization by seawater (large $\Delta^{18}O_{serp\text{-}water}$) or interaction with an ^{18}O-enriched slab derived fluid. More recent work has used Cl and B stable isotope geochemistry to trace serpentinizing fluid sources and infer tectonic setting of serpentinization (Barnes and Sharp, 2006; Barnes et al., 2006, 2009; Benton et al., 2001). For example, isotopic work (O, H, Sr, Li, and B isotopes) on Mariana forearc serpentinites indicates slab-derived fluids as the serpentinizing fluid source (Alt and Shanks, 2006; Benton et al., 2001, 2004; Sakai et al., 1990; Savov et al., 2005, 2007), supporting previous conclusions based on trace element geochemistry.

The purpose of this study is to use stable isotope (O, H, Cl) and major- and trace-element geochemistry to identify serpentinizing fluid sources and unravel the serpentinization history of metasomatized ultramafic rocks from several localities within the Franciscan Complex and Coast Range ophiolite (CRO). The primary focus of this work is the serpentinites within the Franciscan Complex with only a few samples from the CRO included for comparison. The Franciscan Complex has been the location of decades of research, yet little work, particularly geochemistry, has focused on the Franciscan serpentinites. However, these serpentinites may play a critical role in understanding the tectonic history of the Franciscan Complex. For example, several models have been proposed to explain the rapid exhumation rates necessary to explain the lack of complete retrogression observed in high-grade blocks of the Central Belt. One of those group of models invokes exhumation of the high-grade block in a buoyant serpentinite diapir/channel (e.g., Ernst, 1970; Horodyskyj et al., 2009; Moore, 1984). Identifying serpentinizing fluid sources and the location of serpentinization may aid in evaluating these models.

2. Geologic setting and sample locality descriptions

2.1. Overview of the Franciscan Complex and Coast Range ophiolite

The Franciscan Complex of western California and southern Oregon is primarily a shale mélange containing rare low-T, high-P blocks of blueschist, eclogite, and amphibolites, as well as serpentinite blocks, and massive serpentinite slivers (e.g., Bailey et al., 1964; Cloos, 1983, 1986; Ernst, 1970). The Franciscan Complex is a type example of an accretionary wedge that formed during subduction (Bailey and Blake, 1969; Ernst, 1970). The Complex is divided into three north-south trending belts called the Coastal, Central, and Eastern Belts and is overlain by the Coast Range ophiolite and the Great Valley Group (e.g., Bailey and Blake, 1969; Blake et al., 1988; Cloos, 1986; Ernst, 1970; Terabayashi and Maruyama, 1998).

The Middle Jurassic Coast Range ophiolite (CRO; 161–168 Ma) is a >700 km long section of 4–5 km stratigraphically thick dismembered ophiolitic remnants consisting of serpentinized peridotite, pyroxenite, gabbro, diorite, sheeted dike and sill complexes, and submarine lavas overlain by radiolarian chert. In most places the CRO is dismembered and tectonically thinned, representing an incomplete section. The CRO is considered to be basement for the overlying Great Valley Sequence (forearc sedimentary rocks) and in fault contact (Coast Range Fault) with the underlying Franciscan Complex (e.g., Bailey et al., 1970; Coleman, 2000; Hopson et al., 1981, 2008; Shervais et al., 2004, 2005).

2.2. Serpentinites of the Franciscan Complex and Coast Range ophiolite

The best-known and well-studied serpentinites are part of the California Coast Ranges (e.g., CRO, Josephine ophiolite, Trinity ophiolite); however, more poorly studied serpentinites are common within the Franciscan Complex (Coleman, 2000; Wakabayashi, 2004). The CRO stretches from Elder Creek in the north to Point Sal in the south. The CRO is generally thought to have formed in a supra-subduction zone environment (Saleeby, 1982; Shervais, 2001; Shervais and Kimbrough, 1985; Stern and Bloomer, 1992); however, other hypotheses have been proposed such as backarc spreading (e.g., Dickinson et al., 1996) and mid-ocean ridge spreading (e.g., Dickinson et al., 1996; Hopson et al., 1981, 2008). Recent geochemical work suggests that the CRO had a complex history and that a simple supra-subduction model cannot explain all the characteristics (Shervais et al., 2004).

Serpentinite bodies in the Franciscan Complex occur as long slivers (up to 4 km in length and 1 km thick), as smaller blocks, and possibly as sedimentary mélange units (Bailey et al., 1964; King et al., 2003; Loney et al., 1971; Page, 1972; Wakabayashi, 2011a,b). The mechanism for incorporation of the Franciscan serpentinites into the metasedimentary mélange is unclear. One possibility is that the serpentinites were offscraped from metamorphic core complexes as part of the subducting oceanic plate (Coleman, 2000; Wakabayashi, 2004). Alternatively, the serpentinites may be derived from tectonic erosion of the overriding mantle wedge (i.e., blocks from the basal section of the CRO) (Cloos and Shreve, 1988; King et al., 2003; Wakabayashi, 2004) or be sedimentary serpentinites similar to serpentine mud volcanoes found in the forearc (Fryer et al., 2000; Wakabayashi, 2011b). Most of these interpretations are based on possibilities presented from tectonic models and field relationships. Overall, there has been very little work done focusing on the geochemistry of Franciscan serpentinites (Coleman and Keith, 1971; Hirauchi et al., 2008; King et al., 2003; Loney et al., 1971; Page, 1967).

2.3. Sample localities

For the purposes of this study we have concentrated on serpentinite bodies found in the Franciscan Complex. Three samples from/near Cuesta Ridge in the Coast Range ophiolite were also analyzed for comparison (Fig. 1, Table 1). All samples are serpentinized >~95% and consist of lizardite with trace amounts of chrysotile (mineralogy determined by XRD using the Bruker D8 Advance X-Ray Diffractometer at the University of Texas at Austin). Relict pyroxenes are preserved only in sample RM11-4. Relict chromium-rich spinels are present in all samples

Please cite this article as: Barnes, J.D., et al., Petrogenesis of serpentinites from the Franciscan Complex, western California, USA, Lithos (2013), http://dx.doi.org/10.1016/j.lithos.2012.12.018

except highly sheared samples TIB11-1 and TIB11-4, which only contained magnetite.

2.3.1. Franciscan serpentinites

Serpentinite bodies located within the Franciscan Complex mélange have been termed Franciscan serpentinites, rather than associated with the Coast Range ophiolite. However, no contact between serpentinite and host shale matrix was observed for any of the sampled 12 Franciscan serpentinites. In all the cases, the serpentinite outcropped in grassy slopes and the contact was obscured. Samples FS11-1 and FS11-2 are spinel harzburgites from two separate serpentinite outcroppings west of Cuesta Ridge. HWY1 11-1 is a massive spinel harzburgite outcrop from along Hwy. 1 west of Cuesta Ridge. Samples SCT11-1B, C, and D are all from the Sawyer Camp Trail along the San Andreas fault south of San Francisco. Samples SCT11-1B and SCT11-1D are coherent blocks of serpentinized spinel harzburgite within a highly sheared serpentinized peridotite (SCT11-1C). Samples TIB11-1 and TIB11-4 are highly sheared peridotites from Tiburon Peninsula. Nearby samples RM11-2, RM11-3, and RM11-4 are from Ring Mountain. RM11-2 and RM11-3 are slightly to moderately sheared harzburgites and RM11-4 is a blocky spinel lherzolite containing relict clinopyroxene and orthopyroxene. MCR11-3A is a spinel harzburgite from along Mill Creek Road near Healdsburg, California.

2.3.2. Coast Range ophiolite

Cuesta Ridge, near San Luis Obispo, is a dismembered, 25-km long ophiolite sequence (Hopson et al., 1981; Snow, 2002). The lower harzburgite unit is 1 km thick and is cut by rodingitized gabbroic dikes, well exposed along Hwy. 41 (Hsü, 1969; Page, 1972). The serpentinite consists of highly sheared lizardite (Page, 1972). The serpentinized harzburgite is capped by mafic and ultramafic cumulates and finally pillow lava and volcanic breccias (Snow, 2002). Cuesta Ridge has been interpreted to be a SSZ peridotite on the basis of Cr# in spinel (n = 3) and REE patterns in pyroxenes (n = 2) (Choi et al., 2008); however, recent work has noted abyssal affinities in select samples from Cuesta Ridge (Jean et al., 2010; Shervais and Jean, 2012). We sampled two spinel harzburgites from Cuesta Ridge (CR11-2, CR11-3), as well as, one spinel harzburgite from the Hwy. 41 roadcut thought to be a continuation of Cuesta Ridge (HWY41 11-5).

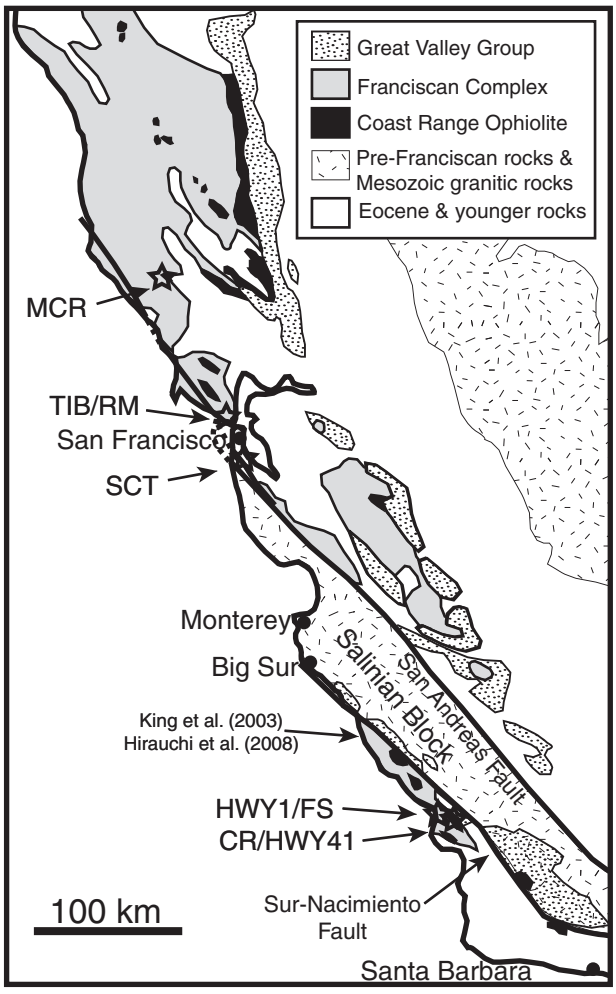

Fig. 1. Geologic map showing serpentinite sample locations (MCR, TIB/RM, SCT, HWY1/FS, CR/HWY41). Locality of the King et al. (2003) and Hirauchi et al. (2008) studies (see text) are noted. Modified from Mehring (2009).

3. Methods

3.1. Major and trace-element geochemistry

Major element geochemical analyses were determined by Actlabs using a lithium metaborate/tetraborate fusion method with subsequent analyses on an ICP-MS. A minimum detection limit of 0.01 wt.% for SiO_2, Al_2O_3, Fe_2O_3, MgO, CaO, Na_2O, K_2O, P_2O_5 and 0.001 wt.% for MnO and TiO_2 is reported. Dilutions for bulk trace element geochemistry was done at the University of Texas at Austin and analysis of the solutions was performed at Rice University using a MC-ICP-MS. Fifty to eighty milligrams of sample, 250 μL HF and 1 mL HNO_3 were loaded into 2.5 mL wrench-top Savillex beakers. Beakers were wrenched down, agitated in an ultrasonic bath for 20 min and heated in a gravity oven at 135 °C overnight. Samples were dried down on a hot plate and the HF/HNO_3 step was repeated. After samples were dried down again, 1 ml of HNO_3 was added, they were agitated for 30 min and heated in an oven at 150 °C for 3 h. Samples were dried down again and the HNO_3 step was repeated. After the four-stage dissolution was complete, two samples (RM11-2 and RM11-4) contained a few small dark brown flecks, presumably spinel. These two samples underwent a third HNO_3 dissolution step. In RM11-4 the flecks disappeared. In RM11-2, only one tiny fleck remained. The contents of the beakers were then diluted up in 125 g of 2% HNO_3 and spiked with Indium to achieve an internal standard at the level of 1 ppb. Analyses at Rice University were performed on a ThermoFinnigan Element 2 magnetic sector ICP-MS. Samples were introduced into the ICP-MS via solution using a 100 microliter/min Elemental Scientific Teflon nebulizer coupled with a cyclonic spray chamber. Most of the trace elements were analyzed in low mass resolution mode. The first series transition metals (V, Cr, Sc, Co, Mn, Fe, Cr, Ni) were analyzed in medium mass resolution mode to avoid isobaric molecular interferences (oxides and argides). Sensitivity in low and mass resolution modes were 10^6 and 10^5 cps/pbb, respectively. USGS basalt standard BHVO-1 was used as an external standard.

Major and minor element compositions of spinel and pyroxene grains were determined using the Cameca JEOL 8200 at the University of Texas at Austin. Single spots were analyzed using a 15 keV accelerating voltage, 20 nA beam current, and a beam size of 20 μm for pyroxenes and 10 nA beam current and a beam size of 5 μm for spinels. Probe standards used were natural Cr-augite (Si, Ca), ilmenite (Mn, Ti), Kakanui augite (Na), chromite (Cr, Fe, Mg, Al) and synthetic Ni-olivine (Ni). A 40s on peak count time was employed for Ni, and the remaining elements had 30 s count times on WDS spectrometers. Chromite and augite standards were analyzed as unknowns to ensure internal consistency. Trace element composition of relict pyroxenes was determined using New Wave UP193FX fast excimer laser

Please cite this article as: Barnes, J.D., et al., Petrogenesis of serpentinites from the Franciscan Complex, western California, USA, Lithos (2013), http://dx.doi.org/10.1016/j.lithos.2012.12.018

Table 1
Sample descriptions and localities.

Sample	Latitude/longitude	Lithostratigraphic unit	Location	Description
CR11-2	N 35°22.604′/W 120°41.496′	Coast Range ophiolite	Cuesta Ridge	Spinel harzburgite
CR11-3	N 35°22.327′/W 120°40.904′	Coast Range ophiolite	Cuesta Ridge	Spinel harzburgite
HWY41 11-5	N 35°25.634′/W 120°45.644′	Coast Range ophiolite	Hwy 41 roadcut near Cuesta Ridge	Spinel harzburgite
HWY1 11-1	N 35°26.483′/W 120°53.432′	Franciscan Complex	Hwy 1 roadcut near Cayuco, CA	Spinel harzburgite
FS11-1	N 35°20.818′/W 120°43.494′	Franciscan Complex	Serpentinite pod west of Cuesta Ridge	Spinel harzburgite
FS11-2	N 35°21.888′/W 120°45.253′	Franciscan Complex	Serpentinite pod west of Cuesta Ridge	Spinel harzburgite
MCR11-3A	N 38°35.685′/W 122°53.853′	Franciscan Complex	Mill Creek Road	Spinel harzburgite
TIB11-1	N 37°53.254′/W 122°27.325′	Franciscan Complex	Tiburon Peninsula	Highly sheared peridotite
TIB11-4	N 37°53.047′/ W 122°27.062′	Franciscan Complex	Tiburon Peninsula	Highly sheared peridotite
RM11-2	N 37°54.591′/W 122°29.062′	Franciscan Complex	Ring Mountain	Spinel harzburgite; slightly sheared
RM11-3	N 37°54.533′/W 122°29.209′	Franciscan Complex	Ring Mountain	Spinel harzburgite; moderately sheared
RM11-4	N 37°54.540′/W 122°29.206′	Franciscan Complex	Ring Mountain	Spinel lherzolite
SCT11-1B	N 37°31.925′/W 122°21.983′	Franciscan Complex	Sawyer Camp Trail	Spinel harzburgite
SCT11-1C	N 37°31.925′/W 122°21.983′	Franciscan Complex	Sawyer Camp Trail	Highly sheared peridotite
SCT11-1D	N 37°31.925′/W 122°21.983′	Franciscan Complex	Sawyer Camp Trail	Spinel harzburgite

ablation system with associated Agilent 7500ce ICP-MS at the University of Texas at Austin. Analysis of clinopyroxene used a 100 μm diameter spot with a dwell time of 30 s at 10 Hz at 30% laser power. Analysis of orthopyroxene used a 100 μm diameter spot with a dwell time of 30 s at 10 Hz at 15% laser power. NIST glass 612 was used as the primary calibration standard. NIST glass 614 and basalt BIR-1G were analyzed as secondary reference standards. Average recoveries among all analytes for these standards using orthopyroxene conditions were 97% and 99%, respectively, and using clinopyroxene analytical conditions were 99% and 89%, respectively, versus GeoREM preferred values. Sample data was reduced based on the SiO_2 content in the pyroxenes obtained from EMPA analysis.

3.2. Stable isotope geochemistry

The extraction and measurement of O, H, and Cl isotopes were done at the University of Texas at Austin. $\delta^{18}O$ values of ~2.0 mg of separated serpentine was measured using the laser fluorination method of Sharp (1990). In order to check for precision and accuracy of oxygen analyses, garnet standard UWG-2 ($\delta^{18}O = +5.8‰$) (Valley et al., 1995), olivine standard San Carlos ($\delta^{18}O = +5.2‰$), and quartz standards Gee Whiz ($\delta^{18}O = +12.6‰$) and Lausanne-1 ($\delta^{18}O = +18.1‰$) were run. All $\delta^{18}O$ values are reported relative to SMOW, where the $\delta^{18}O$ value of NBS-28 is +9.65‰. Precision is ±0.1‰.

δD values of bulk rock powders were determined on ~1 mg of material using the methods of Sharp et al. (2001). The error on each δD analysis is ±2‰. The samples were loaded into silver capsules, which are pyrolized in a ThermoElectron MAT TC-EA (high temperature conversion elemental analyzer). All samples were normalized to biotite standard NBS-30 (δD = −65‰).

Cl isotope methods are based on the procedures of Eggenkamp (1994) and Magenheim et al. (1994) and modified by Barnes and Sharp (2006) and Sharp et al. (2007). Cl^- was released from bulk powdered samples to an aqueous solution by pyrohydrolysis (Magenheim et al., 1994). Cl^- was precipitated from solutions as AgCl via reaction with $AgNO_3$ (Eggenkamp, 1994). Samples were then converted to CH_3Cl and purified of excess CH_3I on a dedicated gas chromatographic system in a continuous He flow before introduction in the mass spectrometer. Precision is ±0.2‰. All stable isotope analyses were made on a ThermoElectron MAT 253 mass spectrometer configured with an H/D collector and an additional collector/matched amplifier system specifically aligned for simultaneous measurement of masses 50 and 52.

4. Results

For ease of presentation of results and discussion, the serpentinites have been divided into 5 groups: 1) Coast Range ophiolite samples from Cuesta Ridge (CR11-2, CR11-3, HWY41 11-5); 2) Franciscan serpentinites west of Cuesta Ridge (FS11-1, FS11-2, HWY1 11-1); 3) Franciscan serpentinites south of San Francisco (SCT11-1B, SCT11-1C, SCT11-1D); 4) Franciscan serpentinites north of San Francisco at Tiburon Peninsula (RM11-2, RM11-3, RM11-4, TIB11-1, TIB11-4); and 5) Franciscan serpentinite near Healdsburg (MCR11-3A).

4.1. Bulk rock geochemistry

All samples have high loss-on ignition (LOI) values (13.8 to 18.5 wt.%) indicative of the extensive serpentinization of the samples. High LOI values also likely reflect the presence of brucite. All samples show refractory major element compositions with high Mg# values (0.881–0.906; $Mg\# = [Mg/(Mg+Fe)]_{molar}$) and low Al_2O_3 and CaO concentrations (0.41 to 2.42 wt.% and 0.03 to 1.01 wt.%, respectively). The highest CaO concentration is in RM11-4, the only sample containing relict clinopyroxene. Cr and Ni concentrations are high, ranging from 901 to 3465 ppm and 1021 to 3653 ppm, respectively.

Serpentinite samples display a wide variation in REE and trace element concentrations and patterns (Figs. 2 and 3). Franciscan serpentinite samples from west of Cuesta Ridge and at Tiburon Peninsula are depleted in LREE compared to HREE ($La_N/Yb_N = 0.13–0.27$ west of Cuesta Ridge and 0.20–0.87 at Tiburon Peninsula with one value at 1.58; $_N$ = C1-chondrite normalized (McDonough and Sun, 1995)) (Fig. 2c, e). The Franciscan serpentinite near Healdsburg, serpentinites south of San Francisco, and one of the three samples from Cuesta Ridge (CR11-3) have slight U-shaped patterns with LREE concentrations higher than the MREE ($La_N/Sm_N = 2.56–5.17$) and even HREE ($La_N/Yb_N = 1.07–2.52$) (Fig. 2b, d, f). The other two samples from the Cuesta Ridge area have nearly flat pattern with sample HWY41-11-5 having the highest MREE concentrations of all samples (Fig. 2b). Trace element patterns normalized to primitive mantle show enrichments in Ba, U, Pb, Sr, and Li in all samples (Fig. 3). All samples also show large enrichments in Ce and Y (Fig. 3). Y/Ho ratios are remarkably high, ranging from 2112-2719.

4.2. Mineral chemistry

Relict pyroxene (both clinopyroxene and orthopyroxene) were found in only one sample, RM11-4. Orthopyroxene has a Mg# value of 0.907 and Al_2O_3 and Cr_2O_3 concentrations of 3.65 wt.% and 0.45 wt.%, respectively. Clinopyroxene has Mg# values of 0.916 to 0.928 and Al_2O_3 and Cr_2O_3 concentrations of 3.74 to 4.98 wt.% and 0.67 to 1.10 wt.%, respectively (Table 3; Fig. 4). Primitive mantle-normalized trace element patterns for clinopyroxenes from RM11-4 are nearly identical and show LREE depletion compared to the higher MREE and

Please cite this article as: Barnes, J.D., et al., Petrogenesis of serpentinites from the Franciscan Complex, western California, USA, Lithos (2013), http://dx.doi.org/10.1016/j.lithos.2012.12.018

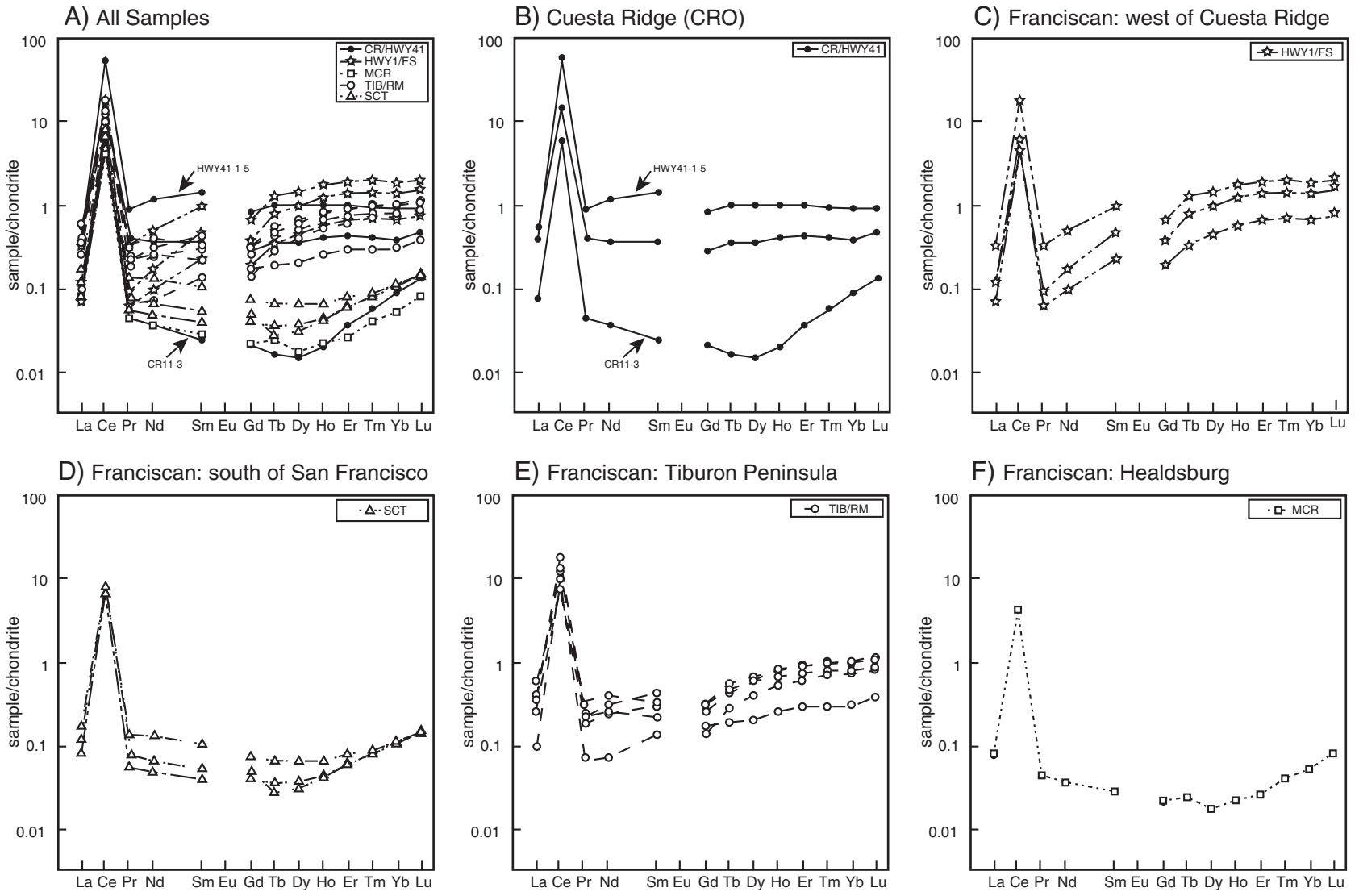

Fig. 2. Chondrite normalized REE compositions of bulk serpentinites from the Franciscan Complex and Coast Range ophiolite. Chondrite normalizing values from McDonough and Sun (1995). A. Compilation of all samples. B. Three CRO samples from Cuesta Ridge. C. Three Franciscan samples from west of Cuesta Ridge. D. Three Franciscan samples from south of San Francisco. E. Five Franciscan samples from Tiburon Peninsula. F. One Franciscan sample from near Healdsburg.

Please cite this article as: Barnes, J.D., et al., Petrogenesis of serpentinites from the Franciscan Complex, western California, USA, Lithos (2013), http://dx.doi.org/10.1016/j.lithos.2012.12.018

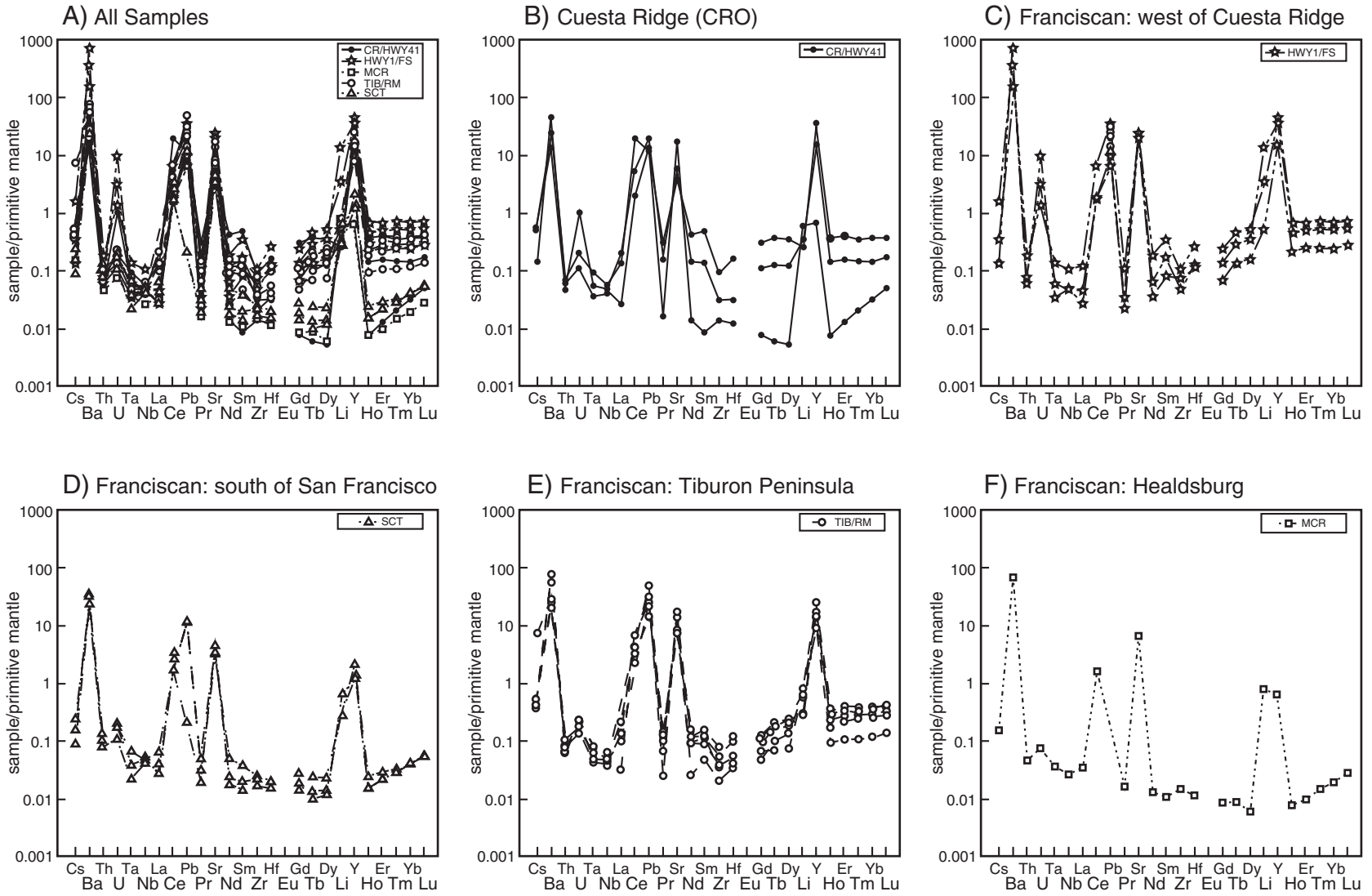

Fig. 3. Primitive mantle normalized trace compositions of bulk serpentinites from the Franciscan Complex and Coast Range ophiolite. Primitive mantle normalizing values from McDonough and Sun (1995). A. Compilation of all samples. B. Three CRO samples from Cuesta Ridge. C. Three Franciscan samples from west of Cuesta Ridge. D. Three Franciscan samples from south of San Francisco. E. Five Franciscan samples from Tiburon Peninsula. F. One Franciscan sample from near Healdsburg.

Please cite this article as: Barnes, J.D., et al., Petrogenesis of serpentinites from the Franciscan Complex, western California, USA, Lithos (2013), http://dx.doi.org/10.1016/j.lithos.2012.12.018

Table 2
Major and trace element composition of serpentinite samples.

	CR11-2	CR11-3	HWY41 11-5	HWY1 11-1	FS11-1	FS11-2	MCR11-3A	TIB11-1	TIB11-4	RM11-2	RM11-3	RM11-4	SCT11-1B	SCT11-1C	SCT11-1D	BHVO-2	BCR
Major elements (*wt.%*)																	
SiO2	40.97	38.87	40.42	40.14		40.55	40.03	42.54	40.71	39.95	40.73	40.19	39.1	39.52	38.72		
Al2O3	0.98	0.43	0.75	2.42		1.47	1.10	1.79	1.77	0.82	1.52	1.76	0.41	0.49	0.59		
Fe2O3(T)	7.88	7.71	7.34	6.34		6.03	7.11	7.45	8.13	8.4	7.76	6.32	7.57	7.45	7.94		
MnO	0.09	0.11	0.11	0.1		0.12	0.13	0.1	0.1	0.11	0.1	0.12	0.12	0.1	0.11		
MgO	34.77	37.41	37.01	34.09		33.68	33.07	33.40	35.36	34.83	33.85	34.76	34.82	34.86	34.36		
CaO	0.04	0.18	0.03	0.49		0.12	0.06	0.05	0.08	0.04	0.34	1.01	0.09	0.05	0.05		
Na2O	0.02	0.02	0.02	0.04		0.02	0.05	0.02	0.02	0.03	0.02	0.06	0.02	0.03	0.03		
K2O	<0.01	<0.01	<0.01	0.04		0.01	0.03	0.01	0.01	<0.01	<0.01	0.02	<0.01	<0.01	<0.01		
TiO2	0.01	0	0.02	0.07		0.02	0.01	0.03	0.04	0.01	0.03	0.03	0	0.01	0.01		
P2O5	<0.01	<0.01	0.01	<0.01		<0.01	0.02	0.02	<0.01	<0.01	<0.01	<0.01	<0.01	<0.01	0.02		
LOI	15.84	14.83	13.80	15.27		16.76	16.26	15.36	13.66	15.56	14.88	13.99	17.33	15.98	18.54		
Total	100.6	99.56	99.52	98.99		98.79	97.88	100.8	99.88	99.75	99.21	98.24	99.46	98.5	100.4		
Mg#	0.887	0.896	0.900	0.906		0.909	0.892	0.889	0.886	0.881	0.886	0.907	0.891	0.893	0.885		
Trace elements (*ppm*)																	
Li	0.546	0.937	0.421	5.48	21.3	0.892	1.26	0.472	0.425	1.04	0.966	0.844	0.810	0.476	0.464	4.46	13.1
Be	0.0267	bdl	0.0232	0.0111	bdl	bdl	bdl	bdl	bdl	bdl	bdl	bdl	bdl	bdl	bdl	1.17	1.64
Sc	6.47	6.27	23.8	12.9	13.7	7.92	6.05	8.33	8.95	7.35	13.4	9.31	7.55	7.43	5.34	31.1	32.5
V	31.5	20.1	45.5	64.7	66.6	36.4	18.1	37.3	37.0	25.9	53.1	43.8	26.1	28.7	26.0	308	414
Cr	2647	1952	2052	2355	2481	2609	901	1793	2057	3465	2808	2106	2763	2531	2539	280	10.1
Co	73.7	96.1	70.3	79.0	110	93.7	112	84.2	84.7	133	101	96.8	100	103	105	44.1	37.6
Ni	2757	2122	1021	1699	2482	2029	2505	1808	1889	3653	2393	2066	2180	2319	2651	119	9.67
Cu	11.1	13.7	16.0	21.7	19.8	19.3	16.3	24.0	19.0	10.9	37.0	28.1	6.14	13.3	11.0	128	16.7
Zn	35.1	35.4	27.3	35.7	48.3	65.4	51.8	31.9	39.1	40.5	42.7	35.4	39.1	34.5	39.5	104	129
Ge	1.03	0.913	1.21	0.842	1.63	1.06	1.33	0.856	1.21	1.02	1.02	0.959	0.922	0.956	1.07	1.63	1.48
Sr	95.8	361	85.1	476	443	396	139	308	150	128	164	369	137	77.0	95.1	395	334
Y	60.9	2.85	130	200	140	64.9	2.71	78.3	98.1	37.5	106	59.5	5.32	5.96	8.88	25.7	36.1
Zr	0.315	0.146	1.05	1.05	0.460	0.792	0.157	0.574	0.770	0.396	0.347	0.226	0.195	0.247	0.266	170	190
Nb	0.0306	0.0283	0.0359	0.0706	0.0334	0.0320	0.0166	0.0291	0.0342	0.0401	0.0379	0.0273	0.0324	0.0349	0.0340	19.2	12.0
Cs	0.0106	0.0113	0.0031	0.0325	0.0076	0.0029	0.0033	0.0076	0.0083	0.0091	0.0106	0.160	0.0032	0.0051	0.0019	0.0927	0.930
Ba	86.8	187	251	2366	946	4702	448	513	307	194	128	246	191	216	236	129	682
La	0.128	0.0178	0.0969	0.0813	0.0296	0.0171	0.0217	0.0624	0.0824	0.0789	0.140	0.0234	0.0193	0.0278	0.0407	15.2	1.16
Ce	9.03	3.30	32.4	10.6	2.75	3.12	2.74	7.94	7.27	9.80	5.34	5.76	4.02	4.06	5.01	37.7	53.6
Pr	0.0366	0.0041	0.0842	0.0292	0.0086	0.0058	0.0043	0.0168	0.0218	0.0215	0.0295	0.0071	0.0052	0.0072	0.0128	5.32	6.81
Nd	0.171	0.0172	0.537	0.224	0.0771	0.0447	0.0173	0.115	0.141	0.114	0.176	0.0331	0.0226	0.0300	0.0600	24.6	28.6
Sm	0.0535	0.0036	0.211	0.142	0.0676	0.0339	0.0042	0.0447	0.0634	0.0340	0.0471	0.0205	0.0057	0.0079	0.0159	6.20	6.55
Gd	0.0581	0.0042	0.171	0.131	0.0756	0.0375	0.0044	0.0507	0.0646	0.0353	0.0613	0.0276	0.0097	0.0080	0.0151	6.00	6.86
Tb	0.0125	0.0006	0.0375	0.0447	0.0285	0.0128	0.0009	0.0153	0.0199	0.0070	0.0175	0.0107	0.0010	0.0013	0.0024	0.947	1.06
Dy	0.0874	0.0037	0.252	0.356	0.237	0.110	0.0042	0.126	0.161	0.0500	0.151	0.0970	0.0077	0.0092	0.0160	5.32	6.32
Ho	0.0224	0.0011	0.0576	0.0940	0.0663	0.0314	0.0012	0.0353	0.0438	0.0141	0.0442	0.0292	0.0023	0.0024	0.0036	0.980	1.28
Er	0.0683	0.0058	0.165	0.297	0.215	0.106	0.0043	0.118	0.144	0.0471	0.149	0.0998	0.0096	0.0096	0.0128	2.53	3.62
Tm	0.0100	0.0014	0.0241	0.0480	0.0349	0.0172	0.0010	0.0192	0.0241	0.0074	0.0249	0.0180	0.0021	0.0020	0.0022	0.343	0.535
Yb	0.0614	0.0143	0.154	0.300	0.221	0.110	0.0086	0.126	0.157	0.0500	0.161	0.117	0.0180	0.0169	0.0181	2.14	3.32
Lu	0.0115	0.0034	0.0238	0.0484	0.0368	0.0193	0.0020	0.0214	0.0260	0.0094	0.0281	0.0200	0.0037	0.0034	0.0036	0.292	0.498
Hf	0.0092	0.0034	0.0484	0.0761	0.0361	0.0323	0.0034	0.0291	0.0367	0.0116	0.0160	0.0110	0.0044	0.0058	0.0056	4.44	4.86
Ta	0.0020	0.0014	0.0034	0.0053	0.0022	0.0014	0.0014	0.0029	0.0031	0.0017	0.0021	0.0017	0.0008	0.0013	0.0019	1.25	0.705
Tl	0.0010	0.0008	bld	0.0492	0.0021	0.0090	0.0014	0.0050	0.0057	0.0026	0.0007	bld	0.0012	0.0018	0.0011	0.0180	0.232
Pb	3.30	2.02	1.44	4.56	1.50	0.994	5.38	3.89	7.37	3.34	1.95	5.24	0.0317	2.16	1.78	1.50	13.5
Th	0.0041	0.0053	0.0058	0.0145	0.0041	0.0052	0.0035	0.0093	0.0068	0.0073	0.0067	0.0066	0.0063	0.0106	0.0075	1.20	5.90
U	0.0218	0.0025	0.0044	0.0271	0.0644	0.202	0.0016	0.0040	0.0041	0.0049	0.0034	0.0030	0.0023	0.0036	0.0037	0.409	1.69
Y/Ho	2719	2591	2257	2128	2112	2067	2258	2218	2240	2660	2398	2038	2313	2483	2467	26	28

bdl = below detection limits.

Table 3
Major and trace element concentrations in relict pyroxene in sample RM11-4.

Major elements (*wt.%*)

	CPX (n=5)	CPX (n=5)	CPX (n=3)	OPX (n=5)
SiO2	52.05	50.74	51.82	54.80
TiO2	0.14	0.16	0.15	0.02
Al2O3	3.74	4.98	3.94	3.65
FeO	2.26	2.57	2.21	6.05
MnO	0.08	0.10	0.09	0.15
MgO	16.45	15.76	15.93	33.10
CaO	23.54	23.31	23.62	0.45
Na2O	0.19	0.22	0.25	bdl
Cr2O3	0.67	1.10	0.77	0.45
NiO	0.04	0.06	0.06	0.07
Total	99.16	99.00	98.84	98.70
Mg#	92.84	91.61	92.79	90.71

Trace elements (*ppm*)

	CPX (n=1)	CPX (n=1)	CPX (n=1)	CPX (n=1)	CPX (n=1)	CPX (n=1)	CPX (n=2)	CPX (n=1)	OPX (n=3)	OPX (n=1)	OPX (n=1)	OPX (n=2)	OPX (n=1)
La	bdl	bdl	bdl	bdl	bdl	bdl	0.12	0.02	bdl	bdl	bdl	0.00	0.04
Ce	bdl	bdl	bdl	bdl	0.00	0.01	0.00	bdl	bdl	bdl	bdl	bdl	bdl
Pr	0.00	0.00	bdl	0.00	0.00	0.00	0.03	0.00	bdl	bdl	bdl	bdl	bdl
Sr	0.87	1.85	1.01	0.70	0.51	0.90	1.19	0.69	1.62	1.54	2.02	3.87	9.38
Nd	0.08	0.07	0.10	0.10	0.10	0.07	0.22	0.11	bdl	bdl	bdl	bdl	bdl
Sm	0.20	0.14	0.15	0.24	0.25	0.24	0.24	0.20	bdl	bdl	bdl	0.02	bdl
Zr	0.19	0.18	0.16	0.24	0.16	0.19	0.19	0.20	0.02	0.02	0.05	0.03	0.07
Eu	0.10	0.07	0.09	0.11	0.08	0.12	0.10	0.10	bdl	bdl	0.02	bdl	bdl
Ti	1087.05	801.73	796.25	1025.70	927.99	944.77	1060.75	866.37	327.72	289.53	447.82	343.50	317.59
Gd	0.61	0.47	0.44	0.66	0.53	0.64	0.62	0.48	bdl	bdl	0.08	0.02	bdl
Tb	0.15	0.11	0.12	0.14	0.13	0.15	0.15	0.12	0.01	0.00	0.03	0.01	bdl
Dy	1.31	0.94	1.05	1.32	1.18	1.33	1.27	0.89	0.05	0.06	0.23	0.09	bdl
Y	8.24	5.96	6.35	8.28	6.90	7.89	7.75	6.13	0.48	0.59	1.97	0.80	0.22
Ho	0.33	0.22	0.25	0.30	0.28	0.29	0.30	0.22	0.02	0.02	0.08	0.03	bdl
Er	1.01	0.72	0.75	1.02	0.85	0.99	0.91	0.69	0.09	0.08	0.26	0.11	bdl
Tm	0.16	0.10	0.13	0.14	0.12	0.14	0.14	0.09	0.01	0.02	0.05	0.03	bdl
Yb	1.00	0.66	0.70	1.00	0.83	0.97	0.90	0.72	0.18	0.20	0.34	0.22	bdl
Lu	0.14	0.09	0.10	0.14	0.13	0.13	0.12	0.09	0.03	0.03	0.07	0.05	bdl

HREE concentrations. Zr is also highly depleted. Orthopyroxene has lower REE concentrations than clinopyroxene with many LREE and MREE below detection limits. HREE concentrentrations are higher than MREE. A negative Zr anomaly is also noted in the orthopyroxene, whereas, Ti concentrations are enriched relative to adjacent REEs (Fig. 5).

Overall, there are limited chemical differences among spinels from an individual sample. Samples from Cuesta Ridge (CR11-2, CR11-3) have Mg# values of 0.441–0.496 and Cr# values of 0.616–0.670. Sample HWY41-11-5 associated with Cuesta Ridge has similar Cr# values (0.663–0.699), but lower Mg# values (0.206–0.309) (Table 4). Franciscan serpentinites west of Cuesta Ridge have Mg# values of 0.647–0.718, but very low Cr# values of 0.144–0.269. Franciscan samples just south of San Francisco have Mg# values of 0.521–0.570 and Cr# values of 0.527–0.655. Samples from Ring Mountain on Tiburon Peninsula have a range of Mg# and Cr# values. One sample (RM11-2) has Mg# values of 0.563–0.603 and Cr# values of 0.493–0.509, whereas, two other samples have slightly higher Mg# values (0.690–0.717) and much lower Cr# values of 0.187–0.226. One Franciscan sample near Healdsburg has Mg# values of 0.486–0.515 and Cr# values of 0.569–0.634 (Table 4).

4.3. Stable isotope geochemistry

Samples from the CRO at the Cuesta Ridge locality have a narrow range of $\delta^{18}O$ values from +6.0 to +6.6‰ and a larger range of $\delta^{37}Cl$ values from +0.4 to +1.7‰. Franciscan serpentinites west of Cuesta Ridge also have a narrow range of $\delta^{18}O$ values from +5.4 to +6.5‰ and $\delta^{37}Cl$ values of +0.2 to +0.3‰. Franciscan serpentinites south of San Francisco have higher $\delta^{18}O$ values from +7.2 to +9.5‰ and $\delta^{37}Cl$ values of −0.1 to 1.2‰. Note, that this set of samples is located on the San Andreas Fault and the sample with the highest $\delta^{18}O$ value and the lowest $\delta^{37}Cl$ value (SCT11-1C) is highly sheared. Franciscan serpentinites from Ring Mountain and Tiburon Peninsula have $\delta^{18}O$ values from +6.0 to +7.3‰ and $\delta^{37}Cl$ values of 0.0 to +0.8‰. One Franciscan serpentinite has a $\delta^{18}O$ value of +7.9‰ and a $\delta^{37}Cl$ value of +0.6‰. δD values of all samples are low, ranging from −107 to −90‰ (Table 5).

5. Discussion

5.1. Stable isotope geochemistry as evidence for serpentinization by seawater

Stable isotope analyses (O, H, Cl) have proven to be excellent tracers of serpentinizing fluid sources, post-serpentinite fluid interaction, and fluid/rock ratios in serpentinites (e.g., Alt and Shanks, 2006; Barnes and Sharp, 2006; Burkhard and O'Neil, 1988; Cartwright and Barnicoat, 1999; Früh-Green et al., 1990, 1996, 2001; Kyser et al., 1999; Sakai et al., 1990; Skelton and Valley, 2000; Yui et al., 1990), allowing one to place some constraints on the tectonic setting of serpentinization. Serpentinites formed by interaction with seawater have predicted $\delta^{18}O$ and δD values shown by the dashed line in Fig. 6 based on the temperature of serpentinization (Saccocia et al., 2009).

Please cite this article as: Barnes, J.D., et al., Petrogenesis of serpentinites from the Franciscan Complex, western California, USA, Lithos (2013), http://dx.doi.org/10.1016/j.lithos.2012.12.018

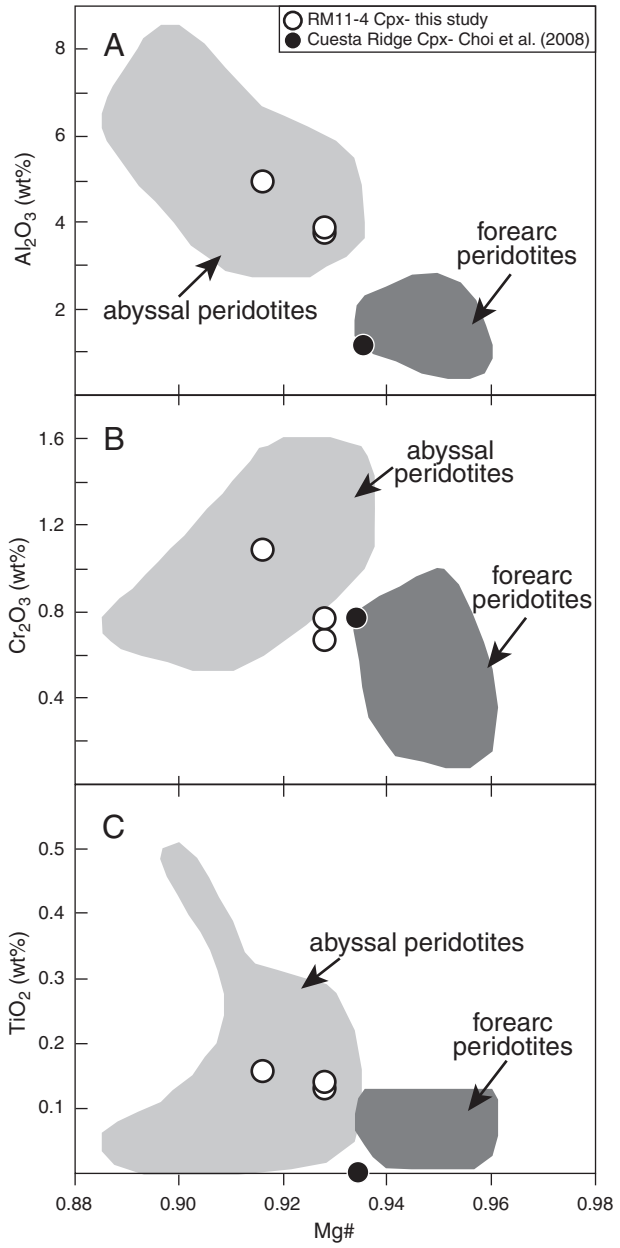

Fig. 4. Minor element compositional plots of clinopyroxene from sample RM11-4 (Tiburon Peninsula). A. Mg# vs. Al_2O_3 (wt.%) B. Mg# vs. Cr_2O_3 (wt.%) C. Mg# vs. TiO_2 (wt.%). Data for compositional fields from Johnson et al. (1990), Hellebrand et al. (2002), Parkinson and Pearce (1998), and Ishii et al. (1992).

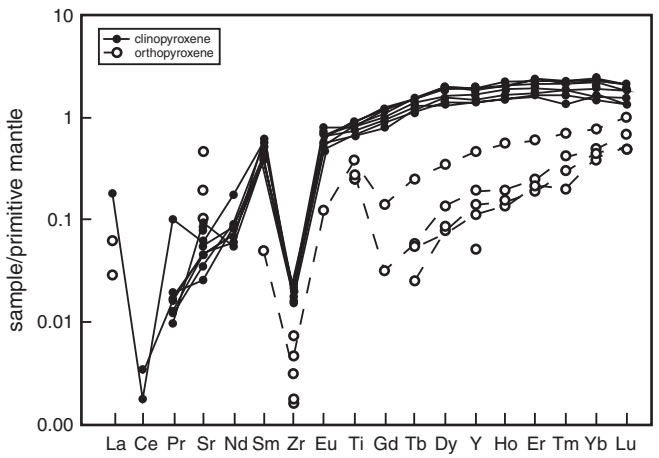

Fig. 5. Primitive mantle normalized REE compositions of clinopyroxene and orthopyroxene from sample RM11-4 (Tiburon Peninsula). Primitive mantle normalizing values from McDonough and Sun (1995).

Previous stable isotope work on serpentinites from the CRO and Franciscan Complex is limited to only a handful of studies and most of which focused on the CRO (King et al., 2003; Magaritz and Taylor, 1976; Taylor and Coleman, 1968; Wenner and Taylor, 1973, 1974). Three stable isotope analyses have been published from Tiburon Peninsula with $\delta^{18}O$ values of +7.6 to +8.1‰ and δD values of −90 to −89‰ (Wenner and Taylor, 1974). King et al. (2003) did a detailed stable isotopic study of a Franciscan serpentinite in a shale matrix mélange at Sand Dollar beach and Jade Cove between Big Sur and HWY1/FS localities on Fig. 1. $\delta^{18}O$ values of olivine (+5.3‰) and clinopyroxene (+5.7‰) in the partially serpentinitized peridotite lie within the range of typical mantle values. Serpentine separates from 5 samples have $\delta^{18}O$ values of +6.3 to +8.1‰. The authors hypothesize that the lherzolite block was incorporated into the subduction channel and metamorphosed by metasomatic fluids at ~450–500 °C, based on isotope thermometry of co-existing calcite and serpentine in veins. The block underwent no metamorphism during its upward path where it was emplaced in a mélange zone that experienced conditions of 150–200 °C and 4–6 kbars (King et al., 2003).

All CRO samples from this study have $\delta^{18}O$ values between +6.0 and +6.6‰. Franciscan serpentinites, with the exception of those on the San Andreas fault (SCT), have $\delta^{18}O$ values of +5.4 to +7.9‰. These $\delta^{18}O$ values are consistent with low-temperature serpentinization by seawater or slightly modified seawater (Fig. 6) (Saccocia et al., 2009). δD values of all samples are low (−107 to −90‰). Although terrestrial serpentinites commonly have low δD values, the reason for these low values remains ambiguous. Authors have suggested interaction with meteoric water, magmatic fluid, and metamorphic fluid as potential mechanisms for low δD values (e.g., Barnes et al., 1967; Burkhard and O'Neil, 1988; Cartwright and Barnicoat, 1999; Früh-Green et al., 2001; Kyser et al., 1999; O'Hanley, 1996; O'Neil and Barnes, 1971). Previous carbon and oxygen stable isotope data of carbonates associated with some Californian serpentinites, as well as ultrabasic fluids issuing from serpentinite hosted springs, have been used to argue for reaction with meteoric water thereby implying some post-emplacement serpentinization (Barnes et al., 1967; O'Neil and Barnes, 1971). The low δD values of Californian serpentinites from this study are consistent with the hypothesis of post-serpentinization, post-emplacement interaction with meteoric water at low temperature. Minor interaction with meteoric waters (e.g., low fluid/rock ratios and low temperature) will lower δD values but not affect O isotope ratios (Burkhard and O'Neil, 1988; Kyser et al., 1999; O'Hanley, 1996) (illustrated by the large hollow arrow in Fig. 6). The high $\delta^{18}O$ values (+7.2 to +9.5‰) and low δD values (−107 to −104‰; lowest values of all the samples) of samples SCT11-1B, -1C, and 1-D (Fig. 6) are likely due to low-T interaction with meteoric water at high fluid–rock ratios due to fluids fluxing through the fault zone. Low-T serpentinization by meteoric waters or low-T meteoric water interaction with high F/R ratios will lead to high $\delta^{18}O$ values (large $\Delta^{18}O_{serp\text{-}water}$) and low δD values (Kyser et al., 1999).

Chlorine isotope measurements of obducted serpentinites and metaperidotites show no Cl isotope fractionation during prograde subduction metamorphism and that the Cl isotope composition of obducted serpentinites is thought to preserve a record of seafloor tectonic processes (Barnes et al., 2006; Bonifacie et al., 2008; John et al., 2011). Serpentinites formed via interaction with seawater have $\delta^{37}Cl$ values of ~+0.2 to +0.5‰ (Barnes and Sharp, 2006). Serpentinites formed from interaction with sedimentary pore fluids and/or sediment-derived fluid have $\delta^{37}Cl$ values of ~−2.0 to −0.5‰ (Barnes and Sharp, 2006; Barnes et al., 2006). Rare serpentinites with $\delta^{37}Cl$ values > +1.0‰ (n = 9) are restricted to serpentine seamounts (n = 2) and obducted serpentinites from Elba Island, Italy

Please cite this article as: Barnes, J.D., et al., Petrogenesis of serpentinites from the Franciscan Complex, western California, USA, Lithos (2013), http://dx.doi.org/10.1016/j.lithos.2012.12.018

Table 4
Composition of spinels from serpentinite samples.

	CR11-2					CR11-3					HWY41 11-5						HWY1 11-1	FS11-2		MCR11-3A				
	S1 (n=2)	S2 (n=2)	S3 (n=2)	S4 (n=1)	S5 (n=1)	S1 (n=2)	S2 (n=2)	S3 (n=2)	S4 (n=1)	S5 (n=1)	S1 (n=1)	S2 (n=1)	S3 (n=1)	S4 (n=1)	S5 (n=1)	S6 (n=1)	S1 (n=1)	S1 (n=1)	S2 (n=1)	S1 (n=2)	S2 (n=2)	S3 (n=2)	S4 (n=2)	S5 (n=2)
SiO2	0.01	0.03	0.03	0.00	bdl	0.01	0.01	0.00	0.01	bdl	0.03	0.02	0.00	0.03	0.04	0.02	0.01	bdl	0.01	0.01	0.03	0.01	0.00	0.01
TiO2	0.03	0.00	0.02	0.03	0.00	bdl	0.02	0.00	0.01	0.01	0.40	0.25	0.11	0.34	0.25	0.28	0.02	0.11	0.05	0.01	0.00	0.00	bdl	bdl
Al2O3	17.79	16.57	18.29	18.44	18.50	18.40	18.80	18.91	19.21	19.08	14.14	13.37	12.62	15.87	13.73	14.46	53.07	42.54	44.11	22.32	18.84	19.48	18.67	18.62
Cr2O3	49.39	50.12	49.37	48.17	48.39	46.92	46.28	46.20	45.88	45.71	41.52	45.79	43.68	43.18	42.99	44.37	13.28	23.39	22.27	43.93	48.13	46.99	48.30	47.61
FeO	20.77	21.15	20.25	21.95	21.77	21.24	20.69	20.98	19.43	21.26	36.21	31.28	34.59	31.88	35.19	31.89	13.28	16.48	15.76	19.94	19.75	20.11	19.30	20.21
NiO	0.08	0.04	0.06	0.00	0.12	0.08	0.07	0.07	0.02	0.05	0.13	0.05	0.06	0.04	0.04	0.00	0.33	0.21	0.19	0.06	0.06	0.08	0.00	0.09
MnO	0.23	0.23	0.20	0.25	0.23	0.28	0.25	0.23	0.22	0.29	0.59	0.44	0.47	0.40	0.56	0.43	0.15	0.19	0.20	0.29	0.30	0.28	0.24	0.30
MgO	10.50	10.82	10.33	9.70	10.15	11.09	11.40	11.40	10.70	10.31	5.27	7.50	6.55	8.00	5.48	7.34	18.93	16.92	17.17	11.20	10.82	10.66	11.52	11.12
CaO	0.00	0.01	0.00	0.01	bdl	0.00	0.01	0.00	0.01	0.00	0.01	0.01	0.01	0.00	bdl	bdl	0.00	0.01	0.01	0.00	0.01	0.01	0.01	0.02
Na2O	bdl	bdl	bdl	0.13	0.00	bdl	bdl	bdl	bdl	bdl	0.05	bdl	0.06	0.03	bdl	0.04	0.01	0.02	bdl	0.03	bdl	0.08	bdl	0.04
Total	98.72	98.86	98.55	98.68	99.14	97.91	97.40	97.76	95.49	96.67	98.37	98.69	98.14	99.77	98.24	98.80	99.07	99.85	99.74	97.80	97.92	97.72	98.01	98.01
Mg#	0.474	0.477	0.476	0.441	0.454	0.482	0.496	0.492	0.495	0.464	0.206	0.299	0.252	0.309	0.217	0.291	0.718	0.647	0.660	0.500	0.494	0.486	0.515	0.495
Cr#	0.651	0.670	0.644	0.637	0.637	0.631	0.623	0.621	0.616	0.616	0.663	0.697	0.699	0.646	0.678	0.673	0.144	0.269	0.253	0.569	0.632	0.618	0.634	0.632

Table 4 (*continued*)

	RM11-2					RM11-3						RM11-4			SCT11-1B						SCT11-1D				
	S1 (n=2)	S2 (n=2)	S3 (n=2)	S4 (n=1)	S5 (n=1)	S1 (n=1)	S2 (n=1)	S3 (n=1)	S4 (n=1)	S5 (n=1)	S6 (n=1)	S1 (n=2)	S2 (n=2)	S3 (n=2)	S1 (n=2)	S2 (n=2)	S3 (n=2)	S4 (n=1)	S5 (n=1)	S6 (n=1)	S1 (n=2)	S2 (n=2)	S3 (n=2)	S4 (n=2)	S5 (n=2)
SiO2	0.00	0.03	0.02	0.03	bdl	0.00	0.00	0.01	bdl	bdl	0.02	0.09	bdl	bdl	0.02	0.02	bdl	0.07	0.01	0.01	0.00	0.00	0.01	0.00	bdl
TiO2	0.03	0.04	0.04	0.02	0.02	0.09	0.01	0.02	0.01	0.11	0.04	0.02	0.01	0.01	0.12	0.09	0.01	bdl	0.06	0.05	0.03	bdl	bdl	bdl	bdl
Al2O3	26.60	26.84	27.10	27.46	26.69	50.26	49.84	48.43	50.37	50.51	49.95	48.39	49.41	47.07	19.11	19.70	18.05	18.76	18.77	19.04	24.17	25.05	24.83	25.22	24.99
Cr2O3	41.19	41.05	40.68	39.87	40.19	17.54	17.60	18.80	17.32	17.50	18.00	18.05	18.01	20.54	49.06	48.78	51.11	49.13	49.40	49.18	42.91	42.17	42.47	41.94	42.35
FeO	17.39	17.55	17.49	18.34	18.46	14.55	14.40	14.75	14.54	14.24	14.47	13.92	13.25	13.26	18.39	18.13	17.45	18.83	18.77	18.79	17.86	17.69	17.78	17.86	17.98
NiO	0.10	0.06	0.09	0.04	0.06	0.18	0.31	0.27	0.34	0.25	0.27	0.25	0.27	0.25	0.12	0.11	0.08	0.05	0.06	0.04	0.05	0.04	0.06	0.10	0.06
MnO	0.21	0.21	0.26	0.23	0.18	0.16	0.14	0.11	0.17	0.13	0.11	0.10	0.14	0.12	0.27	0.22	0.21	0.29	0.25	0.23	0.29	0.24	0.26	0.25	0.23
MgO	14.83	14.51	14.72	14.05	13.36	18.39	18.22	18.40	18.56	18.36	18.32	17.80	18.79	18.78	11.84	11.71	11.82	11.63	11.44	11.50	12.68	12.61	13.23	12.79	12.45
CaO	0.01	0.00	0.01	0.03	0.00	0.02	0.00	0.01	0.00	bdl	bdl	0.01	0.01	0.01	0.02	0.00	bdl	0.04	0.01	0.01	0.01	0.00	0.00	0.01	0.00
Na2O	0.00	0.02	bdl	bdl	bdl	0.02	bdl	bdl	0.01	0.00	0.01	bdl	bdl	bdl	0.05	0.01	0.00	bdl	0.04	0.00	0.01	bdl	bdl	bdl	bdl
Total	100.37	100.30	100.37	100.01	98.87	101.20	100.51	100.79	101.31	101.07	101.19	98.61	99.86	100.02	99.01	98.76	98.70	98.78	98.81	98.85	98.01	97.72	98.53	98.11	97.94
Mg#	0.603	0.596	0.600	0.577	0.563	0.693	0.693	0.690	0.695	0.697	0.693	0.695	0.717	0.716	0.534	0.535	0.547	0.524	0.521	0.522	0.559	0.560	0.570	0.561	0.552
Cr#	0.509	0.506	0.502	0.493	0.502	0.190	0.192	0.207	0.187	0.189	0.195	0.200	0.196	0.226	0.633	0.624	0.655	0.637	0.638	0.634	0.544	0.530	0.534	0.527	0.532

Table 5
Stable isotope composition of Franciscan and Coast Range ophiolite serpentinites.

Sample	$\delta^{18}O$ (‰)	δD (‰)	$\delta^{37}Cl$ (‰)
CR11-2	6.0, 6.2	−95, −97	0.4
CR11-3	6.2, 6.4	−98, −97	1.7
HWY41 11-5	6.6	−93, −93	0.9
HWY1 11-1	6.3, 6.7	−90, −91	0.3
FS11-1	5.4	−90, −90	ND
FS11-2	6.2	−98, −98	0.2
MCR11-3A	7.9	−105, −103	0.5, 0.7
TIB11-1	6.3	−98, −99	0.0, 0.5
TIB11-4	6.9, 7.3	−96, −96	0.8
RM11-2	7.3	−103, −103	0.3
RM11-3	6.0	−99, −100	0.8
RM11-4	6.7	−99, −100	0.6
SCT11-1B	7.2	−107, −107	1.2
SCT11-1C	9.6, 9.3	−104, −104	−0.1, −0.1
SCT11-1D	8.4	−106, −107	0.6

ND = not determined.

(n = 1) and HP/UHP localities in the western Alps (n = 6) (Barnes et al., 2006, 2008; John et al., 2011; Selverstone and Sharp, 2011). Serpentinites with high $\delta^{37}Cl$ values are postulated to reflect a fluid component from the subducted slab, either high-P metasediments or altered oceanic crust (John et al., 2010a; Selverstone and Sharp, 2011). Post-serpentinization interaction with meteoric water does not alter the Cl isotopic composition of serpentinites (Barnes et al., 2006).

All the serpentinites from this study have $\delta^{37}Cl$ values ranging from −0.1 to +1.7‰ with 12 of the 15 samples falling between +0.2 and +0.9‰ (average of all samples = +0.6 ± 0.5‰). These data support serpentinization via seawater on the seafloor. Extreme negative or positive $\delta^{37}Cl$ values reflecting the influence of a non-seawater fluid are not present in the data set, with one exception of CR11-3 at +1.7‰. This highly positive $\delta^{37}Cl$ value at Cuesta Ridge may reflect a subducted slab component, consistent with interpretation of a supra-subduction zone setting.

5.2. Trace elements and Ce and Y anomalies

All serpentinite samples have large enrichments in the fluid-mobile elements, Pb, Sr, Ba, U, and Li, relative to other elements of similar compatibility during mantle melting. This enrichment in FME is commonly observed in serpentinites in both abyssal and forearc settings (Deschamps et al., 2010, 2011; Hattori and Guillot, 2003, 2007; Kodolányа et al., 2012; Li and Lee, 2006; Scambelluri et al., 2004a,b; Vils et al., 2008) due to the high concentrations of these elements in both seawater and slab-derived fluids (Brenan et al., 1995; Keppler, 1996; Manning, 2004). However, enrichments in U are commonly seen in mid-ocean ridge and passive margin settings and not in forearc serpentinites; whereas, Cs and sometimes Sr are more enriched in forearc peridotites compared to those from mid-ocean ridges and passive margins (Kodolányа et al., 2012). None of the serpentinites analyzed show enrichments in Cs with the possible exception of one sample from Tiburon Peninsula. In contrast, all of the samples show enrichments in U (Fig. 3).

Two of the most striking features of the trace element data are the strong relative enrichments in Y and Ce seen in all samples (Fig. 3). Y and Ho are termed so-called geochemical twins due to their identical charge and similar ionic radius, and are therefore not expected to fractionate during high temperature magmatic and metamorphic processes (Blundy and Wood, 2003; Pack et al., 2007). MORB and OIB samples have a range of Y and Ho concentrations, but a near constant Y/Ho ratio of 26–28 identical to the chondritic ratio (Dulski, 2001; Jochum et al., 1986). However, all serpentinite samples from this study have remarkable high Y/Ho ratios (>2000) and Y concentrations ranging from 2.7 to 200 ppm (average = 66.7 ± 59.6 ppm) (Table 2). Note that basalt standards analyzed in this study have Y/Ho ratios of 26–28 lending support to the validity of our analytical analyses (Table 2).

In contrast to silicate melts, Y and Ho have been shown to fractionate in aqueous systems due to chemical complexation and differences in the electron configuration between the two elements (Bau, 1996). Hydrothermal fluids are capable of fractionating Y from Ho at temperatures between 100 and 400 °C (Bau, 1996), temperatures consistent with serpentinization in the lizardite stability field (e.g., Evans, 2004; O'Hanley, 1996). Hydrothermal fluids from a variety of deep-sea vents have Y/Ho ratios of 25 to 50 (Douville et al., 1999). Hydrothermal vein fluorites and marine ferromanganese crusts and nodules have reported Y/Ho ratios up to 200 and 55, respectively, and Y concentrations up to 207 and 481 ppm, respectively (Bau, 1996; Bau and Dulski, 1995; Bau et al., 1996). Interestingly, Ce, like Y, is enriched in ferromanganese crusts and nodules with concentrations ranging from 280 to 1252 ppm (Bau et al., 1996; Nath et al., 1994). Positive Y anomalies, although not to the extreme observed in some of the samples in this study, have been previously documents in two serpentinites from the Feather River Ophiolite, California (Li and Lee, 2006). One of these Feather River Ophiolite samples with a positive Y anomaly is also marked by an extreme negative Ce anomaly (Li and Lee, 2006). Negative Y anomalies relative to Ho have recently been reported in basalt glasses from the Rochambeau Rifts of the Lau Backarc Basin (Jenner et al., 2012). The fractionation of Y from Ho is hypothesized to be from variable assimilation of hydrothermally altered portions of altered arc crust (Jenner et al., 2012).

We speculate that the Ce and Y anomalies observed in the serpentinized peridotites of this study may be the result of highly oxidizing conditions which can fractionate Ce from REEs and possibly Y from Ho. Magnetite is highly common in serpentinites due to the preferential incorporation of Mg rather than Fe into the serpentine structure. This reaction requires the dissociation of water to produce H_2 and an oxidized metal of magnetite (reaction 1 below) or sometimes hematite (reaction 2 below).

$$\underset{\text{olivine}}{6(Mg,Fe)_2SiO_4} + 7\,H_2O = \underset{\text{serpentine}}{3(Mg,Fe)_3Si_2O_5(OH)_4} + \underset{\text{magnetite}}{Fe_3O_4} + H_2 \quad (1)$$

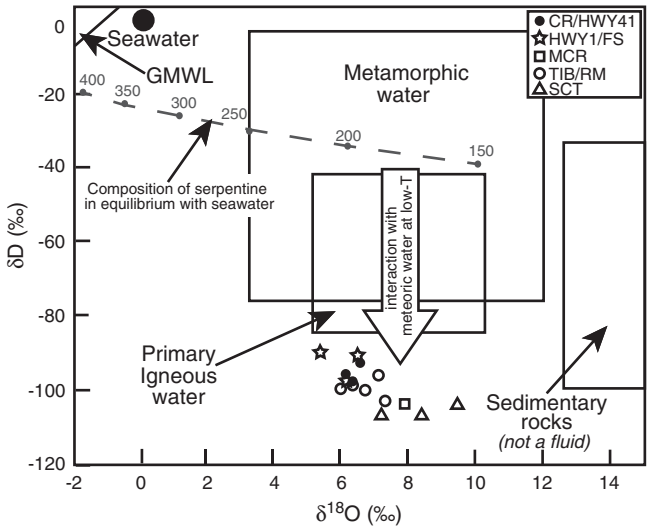

Fig. 6. δD and $\delta^{18}O$ values of various fluids/fluid sources (Sharp, 2007). Dashed line depicts the isotopic composition of serpentinites formed by interaction with seawater at a given temperature using the fractionation factors of Saccocia et al. (2009). Low temperature, post-serpentinization interaction with meteoric water will lower the δD value of serpentinites (e.g., Kyser et al., 1999; O'Hanley, 1996). This process is illustrated by the large hollow arrow.

Please cite this article as: Barnes, J.D., et al., Petrogenesis of serpentinites from the Franciscan Complex, western California, USA, Lithos (2013), http://dx.doi.org/10.1016/j.lithos.2012.12.018

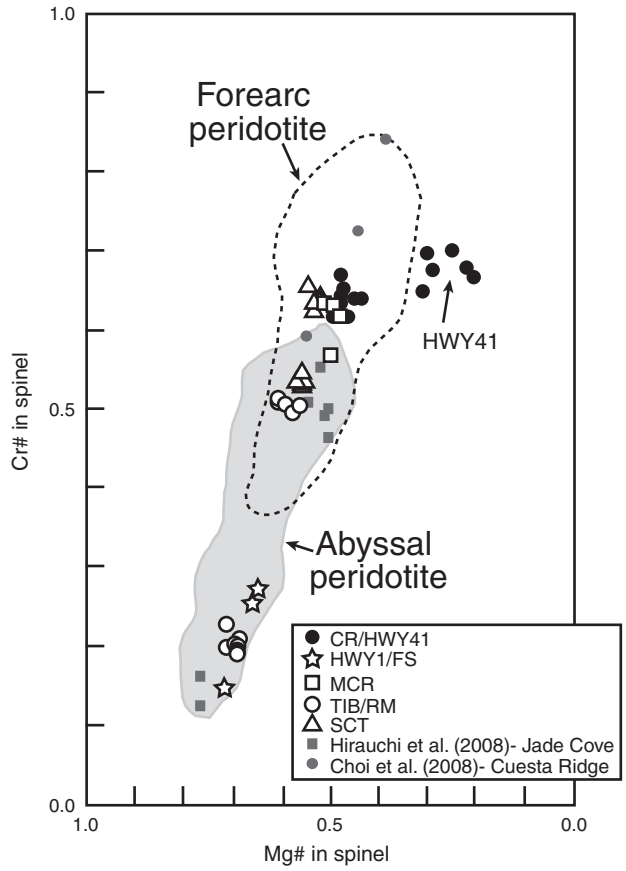

Fig. 7. Mg# vs. Cr# for spinel from Franciscan Complex and Coast Range Ophiolite serpentinites. The compositional fields for abyssal and forearc peridotites are from Tamura and Arai (2006) and references therein.

$$\underset{\text{olivine}}{12(Mg,Fe)_2SiO_4} + 15\,H_2O = \underset{\text{serpentine}}{6(Mg,Fe)_3Si_2O_5(OH)_4} + 3\,\underset{\text{hematite}}{Fe_2O_3} + 3\,H_2 \quad (2)$$

The more oxidized hematite will sequester REEs to a greater degree than magnetite. Hematite will preferentially scavenge Ce (in the +4 valence state) compared to neighboring REEs (in the +3 valence state). Therefore, the resulting Ce/REE and Y/Ho ratios are a product of metal scavenging from hydrothermal fluids at highly oxidizing conditions. Variations in the ratios and the nature of the anomaly (positive or negative) likely depend on the history of the oxidizing fluid throughout the serpentinization process.

5.3. Cuesta Ridge: supra-subduction zone affinity

Cuesta Ridge is part of the CRO that is commonly believed to have formed in a supra-subduction zone setting (Saleeby, 1982; Shervais, 2001; Shervais and Kimbrough, 1985; Snow, 2002; Stern and Bloomer, 1992). Geochemical work on the peridotites from Cuesta Ridge largely supports this interpretation (this study, Choi et al., 2008); however, a few samples from Cuesta Ridge suggest abyssal origin based on REE patterns in pyroxene (Jean et al., 2010). Shervais and Jean (2012) also note enrichments in FME compared to depleted mantle in primary pyroxenes from Cuesta Ridge suggesting the involvement of slab-derived fluids. Choi et al. (2008) report data low Mg# values (0.387 to 0.547) and high Cr# values (0.591 to 0.838) for three spinels from Cuesta Ridge placing them within the forearc peridotite field (Fig. 7). Low TiO_2 (0.00 wt.%), Al_2O_3 (1.26 wt.%) and Cr_2O_3 (0.77 wt.%) concentrations and high Mg# (0.934) place one relict clinopyroxene in the forearc peridotite field (Choi et al., 2008) (Fig. 5). These data are similar to the results found in this study. Spinel data from the two samples from Cuesta Ridge (CR11-2, CR11-3) have low Mg# (0.441 to 0.496) and high Cr# (0.616 to 0.670) also placing them within the forearc peridotite field (Fig. 6). Sample HWY41-11-5 is from a roadcut through Cuesta Ridge and spinel data from this sample plots just outside the field due to lower Mg# values; however the high Cr# values are indicative of forearc peridotites (Fig. 7).

Whole rock REE diagrams for one sample from Cuesta Ridge and the sample from Hwy. 41 show relatively flat profiles (Fig. 2b). These flat REE profiles indicate some enrichment in LREE compared to MREE and HREE either due to melt refertilization in a MOR setting (Niu, 2004; Paulick et al., 2006) or enrichment in LREE in a supra-subduction zone setting (Deschamps et al., 2010; Savov et al., 2005). Sample CR11-3 has overall lower REE concentrations than the other two samples from this locality and a pronounced U-shaped pattern. Boninitic lavas have been documented at Cuesta Ridge (Snow, 2002) and commonly have U-shaped chrondite-normalized REE patterns (Hickey and Frey, 1982). Interaction of the harzbugite with a boninitic melt during initial forearc extension may have resulted in the observed U-shaped REE pattern. Despite the strong positive U anomaly commonly observed in abyssal serpentinites, most of the data from this locality supports a SSZ tectonic setting. The very positive $\delta^{37}Cl$ value of one sample (+1.7‰) and moderately high $\delta^{37}Cl$ value of another (+0.9‰) may also imply some slab-derived fluid component.

5.4. Franciscan Complex serpentinites: mélange containing blocks of abyssal and forearc peridotites

To date, there have been minimal geochemical studies on serpentinites within the Franciscan Complex. Two detailed studies have focused on the serpentinized spinel harzburgites and lherzolites of Sand Dollar beach and Jade Cove (Hirauchi et al., 2008; King et al., 2003). Low Cr# of spinel (0.11 to 0.13) and LREE depletion in clinopyroxenes suggest these serpentinized lherzolites are abyssal peridotites in origin (Hirauchi et al., 2008). Others have argued that Franciscan serpentinites are eroded pieces of the overriding CRO (Cloos and Shreve, 1988; King et al., 2003; Wakabayashi, 2004) or sedimentary serpentinites (Fryer et al., 2000; Wakabayashi, 2011b).

Serpentinite samples from west of Cuesta Ridge have positive sloped REE patterns due to enrichment of HREE over LREE, a typical shape for abyssal peridotites due to melt extraction (Niu, 2004). Spinels from these samples have low Cr# (<0.3) and higher Mg# (>0.6) placing them clearly in the abyssal peridotite field (Fig. 7).

REE patterns for serpentinite samples from Tiburon Peninsula are almost identical to those from west of Cuesta Ridge showing enrichment of HREE over LREE (Fig. 2e). Relict pyroxene from one sample at Tiburon Peninsula shows extreme depletions in LREE concentrations compared to MREE and HREE, similar to those observed in abyssal settings (e.g., Dick and Natland, 1996) (Fig. 5). Major element concentrations also plot within the abyssal field (Fig. 4). Two samples from Tiburon Peninsula have spinels with low Cr# values and plot within the abyssal peridotite field, however, one sample has higher Cr# values and although it still plots within the abyssal field it does overlap with the forearc peridotite field (Fig. 7). Based on the bulk of the data, serpentinites from Tiburon Peninsula likely represent abyssal peridotites that were serpentinized by seawater.

Spinels from sample MCR11-3A, near Healdsburg, plot in the forearc peridote field with one spinel overlapping into both fields (Fig. 7). This sample also has low REE concentrations and a U-shaped chrondite-normalized REE pattern (Fig. 2f) almost identical to that of sample CR11-3 from Cuesta Ridge. The U enrichment in this sample is also relatively minimal. This locality is also close to the Healdsburg ophiolite remanent, interpreted to be part of the

Please cite this article as: Barnes, J.D., et al., Petrogenesis of serpentinites from the Franciscan Complex, western California, USA, Lithos (2013), http://dx.doi.org/10.1016/j.lithos.2012.12.018

CRO (Hopson et al., 1981; Shervais et al., 2004). The proximity to the Healdsburg CRO remanant and the above-described geochemical characteristics imply a possible supra-subduction zone origin.

Franciscan serpentinites from south of San Francisco have slightly higher REE concentrations than the sample near Healdsburg and the one sample from Cuesta Ridge, but a similar U-shaped REE pattern (Fig. 2d). Spinels from this locality all plot within the forearc peridotite field, however, spinels from one of those samples overlaps with that of abyssal peridotites. Based on the bulk REE and the spinel geochemical data, this locality also likely represents eroded pieces of the overriding mantle wedge.

6. Conclusion

The data presented here support the conclusion that Cuesta Ridge, part of the Coast Range ophiolite, formed in a supra-subduction zone setting. Serpentinite blocks within the Franciscan Complex are of mixed origin. Those from Tiburon Peninsula and west of Cuesta Ridge are of abyssal origin and represent offscraped pieces of the subducting slab; whereas, those near Healdsburg and south of San Francisco along the Sawyer Camp Trail are of more ambiguous origin but may represent pieces plucked from the overriding mantle wedge. Stable isotope data is consistent with serpentinization via seawater, however, chlorine isotope data from one sample from Cuesta Ridge could imply a slab-derived fluid component. One striking observation of this study is the large positive Ce and Y anomalies found in all samples. We speculate that these Ce and Y enrichments may be the result of the passage of fluids under oxidizing conditions resulting in the preferential scavenging of Ce and Y by Fe–Mn oxyhydroxides.

Acknowledgments

J.B. thanks M. Cloos for introducing her to the Franciscan Complex and M. Scambelluri and B. Reynard for inviting this contribution. The authors thank B. Byerly for the help with sample preparation and EMP work and property owners on Mill Creek Road for allowing us to take samples. N. Miller is greatly thanked for the assistance with LA-ICP-MS work and discussion. T. Larson is thanked for the help with stable isotope analyses. E. Catlos is thanked for showing us the Sawyer Camp Trail locality. The authors thank J. Shervais and an anonymous reviewer for the improvements to this manuscript. This work was partially supported by funds from the Rosamond Allen Haertlein and Jeanne Allen Ferrin Faculty Fund at the Jackson School of Geosciences

References

Agranier, A., Lee, C.-T.A., Li, Z.-X.A., Leeman, W.P., 2007. Fluid-mobile element budgets in serpentinized oceanic lithospheric mantle: insights from B, As, Li, Pb, PGEs and Os isotopes in the Feather River Ophiolite, California. Chemical Geology 245, 230241.

Alt, J.C., Shanks, W.C., 2006. Stable isotope compositions of serpentinite seamounts in the Mariana forearc: serpentinization processes, fluid sources and sulfur metasomatism. Earth and Planetary Science Letters 242, 272–285.

Augustin, N., Paulick, H., Lackschewitz, K.S., Eisenhauer, A., Garbe-Schönberg, D., Kuhn, T., Botz, R., Schmidt, M., 2012. Alteration at the ultramafic-hosted Logatchev hydrothermal field: constraints from trace element and Sr–O isotope data. Geochemistry, Geophysics, Geosystems 13.

Bailey, E.H., Blake, M.C.J., 1969. Tectonic development of western California during the late Mesozoic. Geotektonika 4, 24–34.

Bailey, E.H., Irwin, W.P., Jones, D.L., 1964. Franciscan and related rocks and their significance in the geology of western California. California Division of Mines and Geology Bulletin 176.

Bailey, E.H., Blake, M.C., Jones, D.L., 1970. Onland Mesozoic oceanic crust in California Coast Ranges. United States Geological Survey Professional Paper 700-C, C70–80.

Barnes, J.D., Sharp, Z.D., 2006. A chlorine isotope study of DSDP/ODP serpentinized ultramafic rocks: insights into the serpentinization process. Chemical Geology 228, 246–265.

Barnes, I., LaMarche, J.V.C., Himmelberg, G., 1967. Geochemical evidence of present-day serpentinization. Science 156, 830–832.

Barnes, J.D., Selverstone, J., Sharp, Z.D., 2006. Chlorine chemistry of serpentinites from Elba, Italy, as an indicator of fluid source and subsequent tectonic history. Geochemistry, Geophysics, Geosystems 7, Q08015. http://dx.doi.org/10.1029/2006GC001296.

Barnes, J.D., Sharp, Z.D., Fischer, T.P., 2008. Chlorine isotope variations across the Izu-Bonin-Mariana arc. Geology 36, 883–886.

Barnes, J.D., Paulick, H., Sharp, Z.D., Bach, W., Beaudoin, G., 2009. Stable isotope ($\delta^{18}O$, δD, $\delta^{37}Cl$) evidence for multiple fluid histories in mid-Atlantic abyssal peridotites (ODP Leg 209). Lithos 110, 83–94.

Bau, M., 1996. Controls on the fractionation of isovalent trace elements in magmatic and aqueous systems: evidence from Y/Ho, Zr/Hf, and lanthanide tetrad effect. Contributions to Mineralogy and Petrology 123, 323–333.

Bau, M., Dulski, P., 1995. Comparative study of yttrium and rare-earth element behaviours in fluorine-rich hydrothermal fluids. Contributions to Mineralogy and Petrology 119, 213–223.

Bau, M., Koschinsky, A., Dulski, P., Hein, J.R., 1996. Comparison of the partitioning behaviours of yttrium, rare earth elements, and titanium between hydrogenetic marine ferromanganese crusts and seawater. Geochimica et Cosmochimica Acta 60, 1709–1725.

Benton, L.D., Ryan, J.G., Tera, F., 2001. Boron isotope systematics of slab fluids as inferred from a serpentine seamount, Mariana forearc. Earth and Planetary Science Letters 187, 273–282.

Benton, L.D., Ryan, J.G., Savov, I.P., 2004. Lithium abundance and isotope systematics of forearc serpentinites, Conical Seamount, Mariana forearc: insights into the mechanics of slab-mantle exchange during subduction. Geochemistry, Geophysics, Geosystems 5, Q08J12. http://dx.doi.org/10.1029/2004GC000708.

Blake, M.C., Jayko, A.S., McLaughlin, R.J., Underwood, M.B., 1988. Metamorphic and tectonic evolution of the Franciscan Complex, northern California. In: Ernst, W.G. (Ed.), Metamorphism and Crustal Evolution of the Western United States. Prentice-Hall, Englewood Cliffs, N.J., pp. 1035–1060.

Blundy, J., Wood, B., 2003. Partitioning of trace elements between crystals and melts. Earth and Planetary Science Letters 210, 383–397.

Bonifacie, M., Busigny, V., Mével, C., Philippot, P., Agrinier, P., Jendrzejewski, N., Scambelluri, M., Javoy, M., 2008. Chlorine isotopic composition in seafloor serpentinites and high-pressure metaperidotites. Insights into oceanic serpentinization and subduction processes. Geochimica et Cosmochimica Acta 72, 126–139.

Brenan, J.M., Shaw, H.F., Ryerson, F.J., 1995. Experimental evidence for the origin of lead enrichment in convergent-margin magmas. Nature 378, 54–56.

Burkhard, D.J.M., O'Neil, J.R., 1988. Contrasting serpentinization processes in the eastern Central Alps. Contributions to Mineralogy and Petrology 99, 498–506.

Cartwright, I., Barnicoat, A.C., 1999. Stable isotope geochemistry of Alpine ophiolites: a window to ocean-floor hydrothermal alteration and constraints on fluid–rock interaction during high-pressure metamorphism. International Journal of Earth Sciences 88 (2), 219–235.

Choi, S.H., Shervais, J.W., Mukasa, S.B., 2008. Supra-subduction and abyssal mantle peridotites of the Coast Range ophiolite, California. Contributions to Mineralogy and Petrology 156, 551–576.

Cloos, M., 1983. Comparative study of melange matrix and metashales from the Franciscan Subduction Complex with the basal Great Valley Sequence, California. Journal of Geology 91, 291–306.

Cloos, M., 1986. Blueschists in the Franciscan Complex of California: petrotectonic constraints on uplift mechanisms. Mem. Geol. Soc. Amer. 77–93.

Cloos, M., Shreve, R.L., 1988. Subduction-channel model of prism accretion, melange formation, sediment subduction, and subduction erosion at convergent plate margins: 2. Implications and discussion. Pure and Applied Geophysics 128, 501–545.

Coleman, R.G., 2000. Prospecting for ophiolites along the California continental margin. In: Dilek, Y., Moores, E.M., Elthon, D., Nicolas, A. (Eds.), Ophiolites and oceanic crust: new insights from field studies and the ocean drilling program: Geological Society of America Special Paper, pp. 351–364 (Boulder, Colorado).

Coleman, R.G., Keith, T.E., 1971. A chemical study of serpentinization – Burro Mountain, California. Journal of Petrology 12, 311–328.

Dai, J.-G., Wang, C.-S., Hébert, R., Santosh, M., Li, Y.-L., Xu, J.-Y., 2011. Petrology and geochemistry of peridotites in the Zhongba ophiolite, Yarlung Zangbo Suture Zone: implications for the Early Cretaceous intra-oceanic subduction zone within the Neo-Tethys. Chemical Geology 288, 133–148.

Deschamps, F., Guillot, S., Godard, M., Chauvel, C., Andreani, M., Hattori, K., 2010. In situ characterization of serpentinites from forearc mantle wedges: timing of serpentinization and behavior of fluid-mobile elements in subduction zones. Chemical Geology 269, 262–277.

Deschamps, F., Guillot, S., Godard, M., Andreani, M., Hattori, K., 2011. Serpentinites act as sponges for fluid-mobile elements in abyssal and subduction zone environments. Terra Nova 23, 171–178.

Dick, H.J.B., Natland, J.H., 1996. Late-stage melt evolution and transport in the shallow mantle beneath the East Pacific Rise. In: Mével, C., Gillis, K.M., Allan, J.F., Meyer, P.S. (Eds.), Proc. ODP, Sci. Results. Ocean Drilling Program, College Station, TX, pp. 103–134.

Dickinson, W.R., Hopson, C.A., Saleeby, J.B., 1996. Alternate origins of the Coast Range ophiolite (California): introduction and implications. GSA Today 6, 1–10.

Dilek, Y., 2003. Ophiolite concepts and its evolution. In: Dilek, Y., Newcomb, S. (Eds.), Ophiolite Concept and the Evolution of Geological Thought. Geological Society of America Special Paper, Boulder, Colorado, pp. 1–16.

Douville, E., Bienvenu, P., Charlou, J.L., Donval, J.P., Fouquet, Y., Appriou, P., Gamo, T., 1999. Yttrium and rare earth elements in fluids from various deep-sea hydrothermal systems. Geochimica et Cosmochimica Acta 63, 627–643.

Douville, E., Charlou, J.L., Oelkers, E.H., Bienvenu, P., Jove Colon, C.F., Donval, J.P., Fouquet, Y., Prieur, D., Appriou, P., 2002. The rainbow vent fluids (36°14′N,

Please cite this article as: Barnes, J.D., et al., Petrogenesis of serpentinites from the Franciscan Complex, western California, USA, Lithos (2013), http://dx.doi.org/10.1016/j.lithos.2012.12.018

MAR): the influence of ultramafic rocks and phase separation on trace metal content in Mid-Atlantic Ridge hydrothermal fluids. Chemical Geology 184, 37–48.
Dulski, P., 2001. Reference materials for geochemical studies: new analytical data by ICP-MS and critical discussion of reference values. Geostandard. Newsl. J. Geostandard. Geoanal. 25, 87–125.
Eggenkamp, H.G.M., 1994. The geochemistry of chlorine isotopes. Ph.D. Thesis, Universiteit Utrecht, 151 pp.
Ernst, W.G., 1970. Tectonic contact between the Franciscan melange and the Great Valley sequence, crustal expression of a Late Mesozoic Benioff zone. Journal of Geophysical Research 75, 886–901.
Evans, B., 2004. The serpentinite multisystem revisited: chrysotile is metastable. International Geology Review 46, 479–506.
Früh-Green, G.L., Weissert, H., Bernoulli, D., 1990. A multiple fluid history recorded in Alpine ophiolites. Journal of the Geological Society 147, 959–970.
Früh-Green, G.L., Plas, A., Lécuyer, C., 1996. Petrologic and stable isotope constraints on hydrothermal alteration and serpentinization of the EPR shallow mantle at Hess Deep (Site 895). In: Mével, C., Gillis, K.M., Allan, J.F., Meyer, P.S. (Eds.), Proc. ODP, Sci. Results. Ocean Drilling Program, College Station, TX, pp. 255–287.
Früh-Green, G.L., Scambelluri, M., Vallis, F., 2001. O–H isotope ratios of high pressure ultramafic rocks: implications for fluid sources and mobility in the subducted hydrous mantle. Contributions to Mineralogy and Petrology 141 (2), 145–159.
Fryer, P., Lockwood, J.P., Becker, N., Phipps, S., Todd, C.S., 2000. Significance of serpentine mud volcanism is convergent margins. In: Dilek, Y., Moores, E.M., Elthon, D., Nicolas, A. (Eds.), Ophiolites and oceanic crust: new insights from field studies and the ocean drilling program: Geological Society of America Special Paper, 349, pp. 35–51 (Boulder, Colorado).
Hattori, K.H., Guillot, S., 2003. Volcanic fronts form as a consequence of serpentinite dehydration in the forearc mantle wedge. Geology 31, 525–528.
Hattori, K.H., Guillot, S., 2007. Geochemical character of serpentinites associated with high- to ultrahigh-pressure metamorphic rocks in the Alps, Cuba, and the Himalayas: recycling of elements in subduction zones. Geochemistry, Geophysics, Geosystems 8.
Hellebrand, E., Snow, J.E., Hoppe, P., Hofmann, A.W., 2002. Garnet field melting and late stage refertilization in residual abyssal peridotites from the Central Indian Ridge. Journal of Petrology 43, 2305–2338.
Hickey, R.L., Frey, F.A., 1982. Geochemical characteristics of boninite series volcanics: implications for their source. Geochimica et Cosmochimica Acta 46, 2099–2115.
Hirauchi, K., Tamura, A., Arai, S., Yamaguchi, H., Hisada, K., 2008. Fertile abyssal peridotites within the Franciscan subduction complex, central California: possible origin as detached remnants of oceanic fracture zones located close to a slow-spreading ridge. Lithos 105, 319–328.
Hopson, C.A., Mattinson, J.M., Pessagno, E.A., 1981. Coast Range ophiolite, western California. In: Ernst, W.G. (Ed.), The Geotectonic Development of California. Prentice-Hall, Englewood Cliffs, New Jersey, pp. 418–510.
Hopson, C.A., Mattinson, J.M., Pessagno, E.A., Luyendyk, B.P., 2008. California Coast Range ophiolite: composite Middle and Late Jurassic oceanic lithosphere. In: Wright, J.E., Shervais, J.W. (Eds.), Ophiolites, Arcs, and Batholiths: A Tribute to Cliff Hopson: Geological Society of America Special Paper, 438, pp. 1–101.
Horodyskyj, U., Lee, C.-T.A., Luffi, P., 2009. Geochemical evidence for exhumation of eclogite via serpentinite channels in ocean-continent subduction zones. Geosphere 5, 426–438.
Hsü, K.J., 1969. Preliminary Report and Geologic Guide to Franciscan Melanges of the Morro Bay-San Simeon area. California Division of Mines and Geology, California, p. 46.
Ishii, T., Robinson, P.T., Maekawa, H., Fiske, R., 1992. Petrological studies of peridotites from diapiric serpentinite seamounts in the Izu-Ogasawara-Mariana forearc. In: Fryer, P., Pearce, J.A., Stokking, L.B. (Eds.), Proc. of the Ocean Drilling Program, Sci. Results. Ocean Drilling Program, College Station, TX, pp. 445–485.
Janecky, D.R., Seyfried, J.W.E., 1986. Hydrothermal serpentinization of peridotite within the oceanic crust: experimental investigations of mineralogy and major element chemistry. Geochimica et Cosmochimica Acta 50, 1357–1378.
Jean, M.M., Shervais, J.W., Choi, S.-H., Mukasa, S.B., 2010. Melt extraction and melt refertilization in mantle peridotite of the Coast Range ophiolite: an LA-ICP-MS study. Contributions to Mineralogy and Petrology 159, 113–136.
Jenner, F.E., Arculus, R.J., Mavrogenes, J.A., Dyriw, N.J., Nebel, O., Hauri, E.H., 2012. Chalcophile element systematics in volcanic glasses from the northwestern Lau Basin. Geochemistry, Geophysics, Geosystems 13, Q06014. http://dx.doi.org/10.1029/2012GC004088.
Jochum, K.P., Seifert, H.M., Spettel, B., Palme, H., 1986. The solar-system abundances of Nb, Ta, and Y, and the relative abundances of refractory lithophile elements in differentiated planetary bodies. Geochimica et Cosmochimica Acta 50, 1173–1183.
John, T., Layne, G.D., Haase, K.M., Barnes, J.D., 2010a. Chlorine isotope evidence for crustal recycling into the Earth's mantle. Earth and Planetary Science Letters 298, 175–182.
John, T., Scherer, E.E., Schenk, V., Herms, P., Halama, R., Garbe-Schönberg, D., 2010b. Subducted seamounts in an eclogite-facies ophiolite sequence: the Andean Raspas Complex, SW Ecuador. Contributions to Mineralogy and Petrology 159, 265–284.
John, T., Scambelluri, M., Frische, M., Barnes, J.D., Bach, W., 2011. Dehydration of subducting serpentinite: implications for halogen mobility in subduction zones and the deep halogen cycle. Earth and Planetary Science Letters. http://dx.doi.org/10.1016/j.epsl.2011.05.038.
Johnson, K.T.M., Dick, H.J.B., Shimizu, N., 1990. Melting in the oceanic upper mantle: an ion microprobe study of diopsides in abyssal peridotites. Journal of Geophysical Research 95, 2661–2678.
Keppler, H., 1996. Constraints from partitioning experiments on the composition of subduction-zone fluids. Nature 380, 237–240.
King, R.L., Kohn, M.J., Eiler, J.M., 2003. Constraints on the petrological structure of the subduction zone slab-mantle interface from Franciscan Complex exotic ultramafic blocks. Geological Society of America Bulletin 115, 1097–1109.
Kodolánya, J., Pettke, T., Spandler, C., Kamber, B.S., Gméling, K., 2012. Geochemistry of ocean floor and fore-arc serpentinites: constraints on the ultramafic input to subduction zones. Journal of Petrology 53, 235–270.
Kyser, T.K., O'Hanley, D.S., Wicks, F.J., 1999. The origin of fluids associated with serpentinization processes: evidence from stable-isotope compositions. The Canadian Mineralogist 37, 223–237.
Li, Z.-X.A., Lee, C.-T.A., 2006. Geochemical investigation of serpentinized oceanic lithospheric mantle in the Feather River Ophiolite, California: implications for the recycling rate of water by subduction. Chemical Geology 235, 161–185.
Loney, R.A., Himmelberg, G.R., Coleman, R.G., 1971. Structure and petrology of the Alpine-type peridotite at Burro Mountain, California, U.S.A. Journal of Petrology 12, 245–309.
Magaritz, M., Taylor, H.P.J., 1976. Oxygen, hydrogen and carbon isotope studies of the Franciscan formation, Coast Ranges, California. Geochimica et Cosmochimica Acta 40, 215–234.
Magenheim, A.J., Spivack, A.J., Volpe, C., Ransom, B., 1994. Precise determination of stable chlorine isotopic ratios in low-concentration natural samples. Geochimica Et Cosmochimica Acta 58 (14), 3117–3121.
Manning, C.E., 2004. The chemistry of subduction-zone fluids. Earth and Planetary Science Letters 223, 1–16.
McDonough, W.F., Sun, S.S., 1995. The composition of the Earth. Chemical Geology 120 (223–253).
Mehring, P.M., 2009. Petrology of the Coast Range Ophiolite near San Simeon, California: implications for tectonic setting. University of Texas at Austin, Austin, Texas (353 pp.).
Mével, C., 2003. Serpentinization of abyssal peridotites at mid-ocean ridges. C. R. Geoscience 335, 825–852.
Moore, D.E., 1984. Metamorphic history of a high-grade blueschist exotic block from the Franciscan Complex, California. Journal of Petrology 25, 126–150.
Nath, B.N., Roelandts, I., Sudhakar, M., Plüger, W.L., Balaram, V., 1994. Cerium anomaly variations in ferromanganese nodules and crusts from the Indian Ocean. Marine Geology 120, 385–400.
Niu, Y., 2004. Bulk-rock major and trace-element compositions of abyssal peridotites: implications for mantle melting, melt extraction and post-melting processes beneath mid-ocean ridges. Journal of Petrology 45, 2423–2458.
O'Hanley, D.S., 1996. Serpentinites: Records of Tectonic and Petrological History. Oxford University Press, New York (277 pp.).
O'Neil, J.R., Barnes, I., 1971. C^{13} and O^{18} compositions in some fresh-water carbonates associated with ultramafic rocks and serpentinites: western United States. Geochimica et Cosmochimica Acta 35, 687–697.
Pack, A., Russell, S.S., Shelley, J.M.G., van Zuilen, M., 2007. Geo- and cosmochemistry of the twin elements yttrium and holmium. Geochimica et Cosmochimica Acta 71, 4592–4608.
Page, N.J., 1967. Serpentinization at Burro Mountain. California Contributions to Mineralogy and Petrology 14, 321–342.
Page, B.M., 1972. Oceanic crust and mantle fragment in subduction complex near San Luis Obispo, California. Geological Society of America Bulletin 83, 957–972.
Parkinson, I.J., Pearce, J.A., 1998. Peridotites from the Izu-Bonin-Mariana forearc (ODP Leg 125): evidence for mantle melting and melt-mantle interaction in a supra-subduction zone setting. Journal of Petrology 39, 1577–1618.
Paulick, H., Bach, W., Godard, M., De Hoog, J.C.M., Suhr, G., Harvey, J., 2006. Geochemistry of abyssal peridotites (Mid-Atlantic Ridge, 15°20′N, ODP Leg 209): implications for fluid/rock interaction in slow spreading environments. Chemical Geology 234, 179–210.
Ranero, C.R., Morgan, J.P., McIntosh, K., Reichert, C., 2003. Bending-related faulting and mantle serpentinization at the Middle America trench. Nature 425, 367–373.
Saccocia, P.J., Seewald, J.S., Shanks, W.C., 2009. Oxygen and hydrogen isotope fractionation in the serpentine-water and talc-water systems from 250 ° to 450 °C, 50 MPa. Geochimica et Cosmochimica Acta 73, 6789–6804.
Sakai, R., Kusakabe, M., Noto, M., Ishii, T., 1990. Origin of waters responsible for serpentinization of the Izu-Ogasawara-Mariana forearc seamounts in view of hydrogen and oxygen isotope ratios. Earth and Planetary Science Letters 100, 291–303.
Saleeby, J.B., 1982. Polygenetic ophiolite belt of the California Sierra Nevada: geochronological and tectonostratigraphic development. Journal of Geophysical Research B87, 1803–1824.
Savov, I.P., Ryan, J.G., D'Antonio, M., 2005. Geochemistry of serpentinized peridotites from the Mariana forearc Conical seamounts, ODP Leg 125: implications for the elemental recyclng at subduction zones. In: Kelley, K., Mattie, P. (Eds.), Geochemistry, Geophysics, Geosystems 6.
Savov, I.P., Ryan, J.G., D'Antonio, M., Fryer, P., 2007. Shallow slab fluid release across and along the Mariana arc-basin system: insights from geochemistry of serpentinized peridotites from the Mariana fore arc. Journal of Geophysical Research 112.
Scambelluri, M., Fiebig, J., Malaspina, N., Müntener, O., Pettke, T., 2004a. Serpentinite subduction: implications for fluid processes and trace-element recycling. International Geology Review 46, 595–613.
Scambelluri, M., Müntener, O., Ottolini, L., Pettke, T.T., Vannucci, R., 2004b. The fate of B, Cl and Li in the subducted oceanic mantle and in the antigorite breakdown fluids. Earth and Planetary Science Letters 222, 217–234.
Selverstone, J., Sharp, Z.D., 2011. Chlorine isotope evidence for multicomponent mantle metasomatism in the Ivrea Zone. Earth and Planetary Science Letters 310, 429–440.
Sharp, Z.D., 1990. A laser-based microanalytical method for the *in situ* determination of oxygen isotope ratios of silicates and oxides. Geochimica et Cosmochimica Acta 54, 1353–1357.

Please cite this article as: Barnes, J.D., et al., Petrogenesis of serpentinites from the Franciscan Complex, western California, USA, Lithos (2013), http://dx.doi.org/10.1016/j.lithos.2012.12.018

Sharp, Z.D., 2007. Principles of Stable Isotope Geochemistry. Pearson Prentice Hall, Upper Saddle River, NJ (344 pp.).
Sharp, Z.D., Atudorei, V., Durakiewicz, T., 2001. A rapid method for determination of hydrogen and oxygen isotope ratios from water and solid hydrous substances. Chemical Geology 178, 197–210.
Sharp, Z.D., Barnes, J.D., Brearley, A.J., Chaussidon, M., Fischer, T.P., Kamenetsky, V.S., 2007. Chlorine isotope homogeneity of the mantle, crust and carbonaceous chondrites. Nature 446, 1062–1065.
Shervais, J.W., 2001. Birth, death, and resurrection: the life cycle of suprasubduction zone ophiolites. Geochemistry, Geophysics, Geosystems 2.
Shervais, J.W., Jean, M.M., 2012. Inside the subduction factory: modeling fluid mobile element enrichment in the mantle wedge above a subduction zone. Geochimica et Cosmochimica Acta 95, 270–285.
Shervais, J.W., Kimbrough, D.L., 1985. Geochemical evidence for the tectonic setting of the Coast Range ophiolite: a composite island arc-oceanic crust terrane in western California. Geology 13, 35–38.
Shervais, J.W., Kimbrough, D.L., Renne, P., Hanan, B.B., Murchey, B., Snow, C.A., Zoglman Schuman, M.M., Beaman, J., 2004. Multi-stage origin of the Coast Range ophiolite, California: implications for the life cycle of supra-subduction zone ophiolites. International Geology Review 46, 289–315.
Shervais, J.W., Kolesar, P., Andreasen, K., 2005. A field and chemical study of serpentinization- Stonyford, California: chemical flux and mass balance. International Geology Review 47, 1–23.
Skelton, A.D.L., Valley, J.W., 2000. The relative timing of serpentinisation and mantle exhumation at the ocean-continent transition, Iberia: constraints from oxygen isotopes. Earth and Planetary Science Letters 178, 327–338.
Snow, C.A., 2002. Geology of the Cuesta Ridge Ophiolite Remnant near San Luis Obispo, California. Evidence for the Tectonic Setting and Origin of the Coast Range Ophiolite, Utah State University, Logan, Utah. (150 pp.).
Snow, J.E., Dick, H.J.B., 1995. Pervasive magnesium loss by marine weathering of peridotite. Geochimica et Cosmochimica Acta 59, 4219–4235.
Stern, R.J., Bloomer, S.H., 1992. Subduction zone infancy: examples from the Eocene Izu-Bonin-Mariana and Jurassic California arcs. Geological Society of America Bulletin 101, 401–413.
Tamura, A., Arai, S., 2006. Harzburgite-dunite-orthopyroxenite suite as a record of supra-subduction zone setting for the Oman ophiolite mantle. Lithos 90, 43–56.
Taylor, H.P.J., Coleman, R.G., 1968. O^{18}/O^{16} ratios of coexisting minerals in glaucophane-bearing metamorphic rocks. Geological Society of America Bulletin 79, 1727–1756.
Terabayashi, M., Maruyama, S., 1998. Large pressure gap between the Coastal and Central Franciscan belts, northern and central California. Tectonophysics 285, 87–101.
Tonarini, S., Scambelluri, M., 2010. Boron and strontium isotope systematics in deeply subducted alpine-serpentinties: evidence of high-^{11}B fluid flow. Geophysical Research Abstracts 12 (EGU2010-4451).
Valley, J.W., Kitchen, N., Kohn, M.J., Neindorf, C.R., Spicuzza, M.J., 1995. UWG-2, a garnet standard for oxygen isotope ratios: strategies for high precision and accuracy with laser heating. Geochimica et Cosmochimica Acta 59, 5223–5231.
Vils, F., Pelletier, L., Kalt, A., Müntener, O., Ludwig, T., 2008. The lithium, boron and beryllium content of serpentinized peridotites from ODP Leg 209 (Sites 1272A and 1274A): implications for lithium and boron budgets of oceanic lithosphere. Geochimica et Cosmochimica Acta 72, 5475–5504.
Vils, F., Tonarini, S., Kalt, A., Seitz, H.-M., 2009. Boron, lithium and strontium isotopes as tracers of seawater-serpentinite interaction at Mid-Atlantic ridge, ODP Leg 209. Earth and Planetary Science Letters 286, 414–425.
Wakabayashi, J., 2004. Contrasting settings of serpentinties bodies, San Francisco Bay area, California: derivation from the subducting plate vs. mantle hanging wall? International Geology Review 46, 1103–1118.
Wakabayashi, J., 2011a. Subducted sedimentary serpentinite mélanges: record of multiple burial-exhumation cycles and subduction erosion. Tectonophysics. http://dx.doi.org/10.1016/j.tecto.2011.11.006.
Wakabayashi, J., 2011b. Mélanges of the Franciscan Complex, California: diverse structureal settings, evidence for sedimentary mixing, and their connection to subduction processes. In: Wakabayashi, J., Dilek, Y. (Eds.), Mélanges: Processes of Formation and Societal Significance: Geological Society of America Special Paper, pp. 117–141.
Wenner, D.B., Taylor, H.P.J., 1973. Oxygen and hydrogen isotopic studies of the serpentinization of ultramafic rocks in oceanic environments and continental ophiolite complexes. American Journal of Science 273, 207–239.
Wenner, D.B., Taylor, J.H.P., 1974. D/H and O^{18}/O^{16} studies of serpentinization of ultramafic rocks. Geochimica et Cosmochimica Acta 38, 1255–1286.
Yui, T.-F., Yeh, H.-W., Lee, C.W., 1990. A stable isotope study of serpentinization in the Fengtien ophiolite, Taiwan. Geochimica et Cosmochimica Acta 54, 1417–1426.

Please cite this article as: Barnes, J.D., et al., Petrogenesis of serpentinites from the Franciscan Complex, western California, USA, Lithos (2013), http://dx.doi.org/10.1016/j.lithos.2012.12.018